Halide-selective, proton-coupled anion transport by phenylthiosemicarbazones†

Ethan N.W. Howe,[a¶] Vai-Vai Tiffany Chang,[a,b] Xin Wu,[a] William Lewis,[a] Lauren K. Macreadie,[a] and Philip A. Gale*[a,c]

[a] School of Chemistry (F11), The University of Sydney, NSW 2006, Australia.

[b]Chemistry, University of Southampton, Southampton SO17 1BJ, UK.

[c]The University of Sydney Nano Institute (Sydney Nano), The University of Sydney, NSW 2006, Australia.

[¶]Present address: GlaxoSmithKline, GSK Jurong, 1 Pioneer Sector 1, Singapore 628413

*philip.gale@sydney.edu.au

[†]Dedicated to Professor Lechosław Latos-Grażyński on the occasion of his 70th birthday.

Keywords: Anion transport; Hydrogen bonding; Thiosemicarbazones; Switchable receptors

Highlights

• A new class of phenylthiosemicarbazone-based anion receptors have been synthesized and shown to function as pH-switchable transmembrane anion transporters.

• An intramolecular hydrogen bond locks the thiourea binding site and inhibits chloride/nitrate exchange at pH 7.2. Protonation of phenylthiosemicarbazones at pH 4.5 switches on chloride/nitrate exchange activity.

• Anion transport selectivity analysis reveals strong halide over oxyanion preference exhibited by protonated phenylthiosemicarbazones.

• The pH-switchable chloride/nitrate exchange is shown to originate from inhibition of rate-limiting nitrate transport at pH 7.2.

Abstract: Phenylthiosemicarbazones (PTSCs) are proton-coupled anion transporters with pH-switchable behaviour known to be regulated by an imine protonation equilibrium. Previously, chloride/nitrate exchange by PTSCs was found to be inactive at pH 7.2 due to locking of the thiourea anion binding site by an intramolecular hydrogen bond, and switched ON upon imine protonation at pH 4.5. The rate-determining process of the pH switch, however, was not examined. We here develop a new series of PTSCs and demonstrate their conformational behaviour by X-ray crystallographic analysis and pH-switchable anion transport properties by liposomal assays. We report the surprising finding that these compounds are extremely selective for halides over oxyanions in membrane transport. Owing to the high chloride over nitrate selectivity, the pH-dependent chloride/nitrate exchange of PTSCs originates from the rate-limiting nitrate transport process being inhibited at neutral pH, whereas chloride transport remains efficient under both neutral and acidic conditions.

1. Introduction

Small-molecule transmembrane anion transporters are promising anti-cancer drug candidates due to their ability to disrupt pH/anion gradients and membrane potential across cell membranes and in organelles.[1, 2] The research of synthetic anion transporters was initially inspired by the natural product prodigiosin which facilitates efficient H^+/Cl^- symport and as a result neutralizes acidic pH

inside vacuolar organelles including lysosomes, endosomes and Golgi apparatus.[3-5] While prodigiosin exhibits potent anion transport activity under both neutral and acidic conditions, synthetic anion transporters with pH-dependent transport activities have been design with a potential to target the acidic intracellular environment of tumours and reduce the toxicity towards normal cells.[6-10]

Phenylthiosemicarbazones (PTSCs) are a class of pH-switchable anion transporters previously reported to exhibit up to 640-fold increase in chloride/nitrate exchange activity on going from pH 7.2 to 4.0.[11] This pH dependence was regulated by protonation of the imine nitrogen at acidic pH, which led to a conformational switch of the thiourea motif from an inactive *anti*-conformation to an active anion binding *syn*-conformation (Fig. 1a). For a better understanding of anion transport and pH switching mechanism of this class of transporters, we decided to study an expanded library of PTSCs and here report our serendipitous discovery of their extremely high halide over oxyanion transport selectivity leading to the pH-switchable chloride/nitrate exchange being regulated by the rate-limiting nitrate transport process.

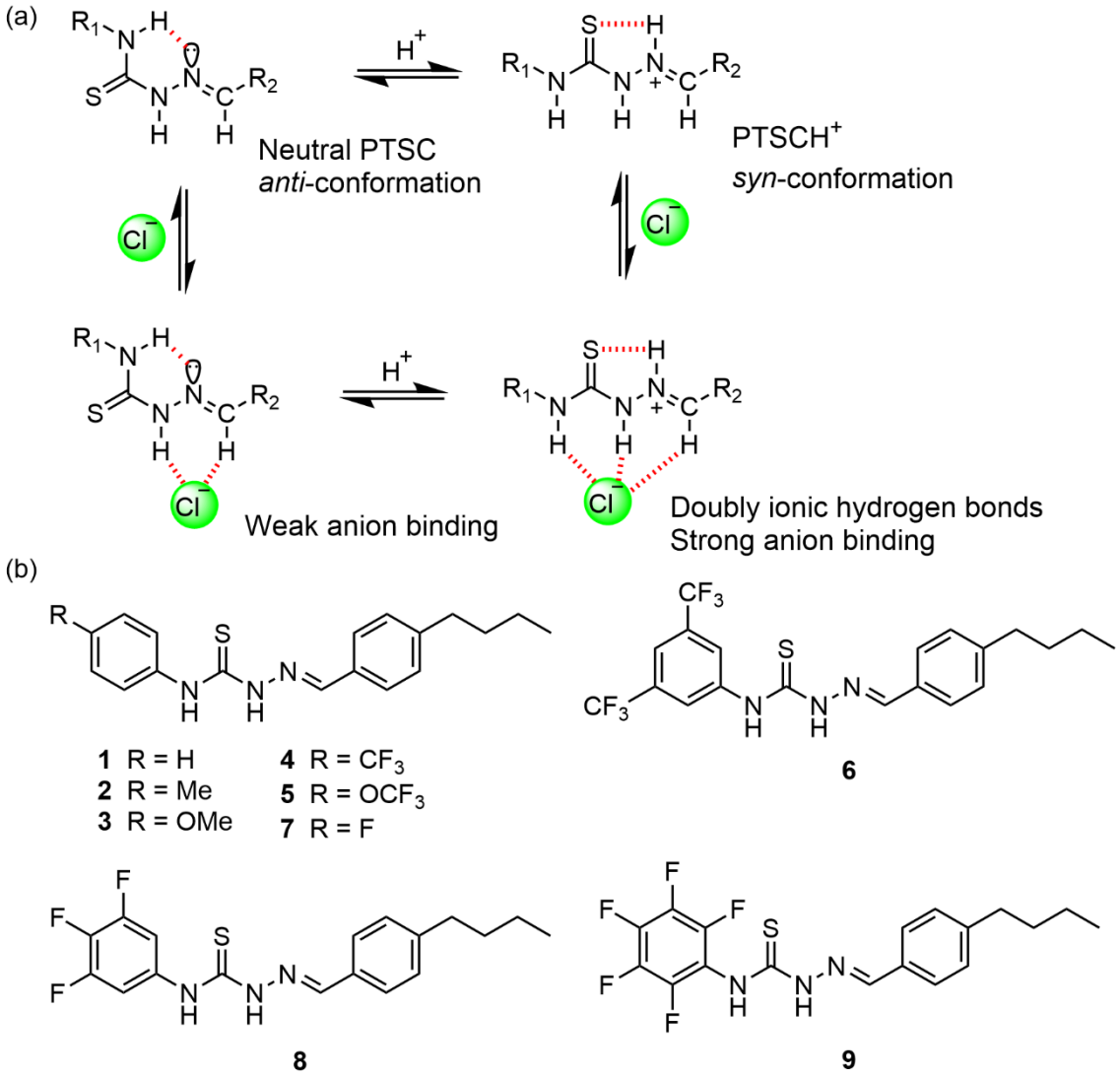

Fig. 1. (a) Mechanism for pH-switchable anion binding by phenylthiosemicarbazones (PTSCs). (b) Structures of new PTSC transporters **1**–**9**.

2. Experimental section

2.1 Materials

All chemicals and solvents were purchased from commercial sources (Alfa Aesar, Fisher Scientific and Sigma Aldrich). 1-Palmitoyl-2-oleoyl-*sn*-glycero-3-phosphocholine (POPC) was purchased from Corden Pharma GmbH. All deuterated solvents for NMR were purchased from Cambridge Isotope Laboratories. Commercially available reagent grade chemicals were used without further purification unless otherwise specified.

2.2 Instruments

^{1}H and ^{13}C NMR spectra were recorded on Bruker Avance AVII400 and AVIIIHD400 FT-NMR spectrometers with 5 mm BBFO z-gradient probes, operating at a frequency of 400 MHz for ^{1}H NMR and 101 MHz for ^{13}C NMR respectively.

LR-MS samples were analysed using a Bruker amaZon SL mass spectrometer equipped with a quadrupole analyser. Samples were introduced to the mass spectrometer via direct injection. Low resolution mass spectra were recorded using positive/negative ion electrospray ionization.

Fluorescence measurements were performed using an Agilent Cary Eclipse Fluorescence Spectrophotometer equipped with a stirrer plate and a temperature controller.

X-ray diffraction data were collected at 100 K on a SuperNova Dual, Cu at home/near Atlas diffractometer.

2.3 Syntheses

The respective substituted *N*-phenyl thiosemicarbazide (~300 mg) was suspended in absolute ethanol (10 mL) and the mixture was treated with 4-butylbenzaldehyde (~1.1 equivalent) and stirred at room temperature under nitrogen atmosphere for > 8 h. The products were re-precipitated with a suitable solvent and were collected by filtration. Characterization data for transporters **1**–**9** is provided in Supplemental Material.

2.4 Crystallographic analysis

The solutions of X-ray diffraction data for transporter **1** were obtained by direct methods using SHELXT[12] followed by successive refinements using full matrix least squares method against F^2 using SHELXL-2018/3.[13] The program OLEX2 [14] was used was used as a graphical SHELX interface. See Supplemental Material for crystal and data refinement parameters.

2.5 Membrane transport assays

Large unilamellar vesicles of POPC were prepared by hydrating a lipid film using an internal solution, followed by 9 freeze-thaw cycles and extrusion 25 times through a 200 nm polycarbonate membrane. Finally, the vesicles were subject to dialysis or Sephadex size-exclusion chromatography using the required external solution to remove unencapsulated chloride ions (ISE assay) or the fluorescence pH indicator 8-hydroxypyrene-1,3,6-trisulfonate (HPTS assay) to obtain vesicle stock suspensions for membrane transport studies.

The vesicles stock suspensions were diluted to POPC concentrations of 1 mM (ISE assay) and 0.1 mM using the required external solution. DMSO solutions of transporters were added to the vesicle suspensions and the membrane transport kinetics was studied by measuring the chloride concentrations in the external solutions using a chloride selective electrode (ISE assay) or by monitoring the ratiometric fluorescence response from intravesicular pH indicator HPTS (HPTS assay). See Supplemental Material for detailed assay conditions.

3. Results and Discussion

3.1 Synthesis of anion transporters **1**–**9** and crystallographic analysis of **1**

Transporters **1**–**9** bearing aryl substituents on both sides of the PTSC core were synthesized by imine condensation of 4-pentylbenzaldehyde with the corresponding phenylthiosemicarbazide. Single crystals of transporter **1** (CCDC 2103182) of suitable quality for X-ray diffraction were obtained *via* slow evaporation of a DMSO solution. Tranporter **1** crystallizes in the monoclinic space group $P2_1/c$ with two formula units in the asymmetric unit. The crystal structure highlights the thione form to be predominant due to the CS bond lengths (1.6869(18) Å and 1.6788(19) Å) and the C=N–N angles (116.15(16)° and 114.90(16)°) being similar to other thione tautomeric structures. The presence of two NH and one carbazone CH hydrogen-bond donor group, permits the formation of multiple hydrogen bonds between pairs of **1**.

Each pair is held together through phenyl ring edge-to-face C–H···π stacking interactions between aromatic rings (3.2106(10) Å and 3.295(10) Å). Close C(13)–H···N(6) (3.570(3) Å) and C(5)–H···S(2) (3.677(2) Å) interactions further stabilise the pairs of receptors. Pairs run parallel along the a-axis, 180° to one another, held together through close hydrogen bonding interactions between the thiosemicarbazone groups. The $R_2^2(6)$ and $R_2^2(8)$ motifs present between the carbazone groups of adjacent pairs necessitates their parallel position. Overall, this arrangement forms 2D sheets running along the ab axis.

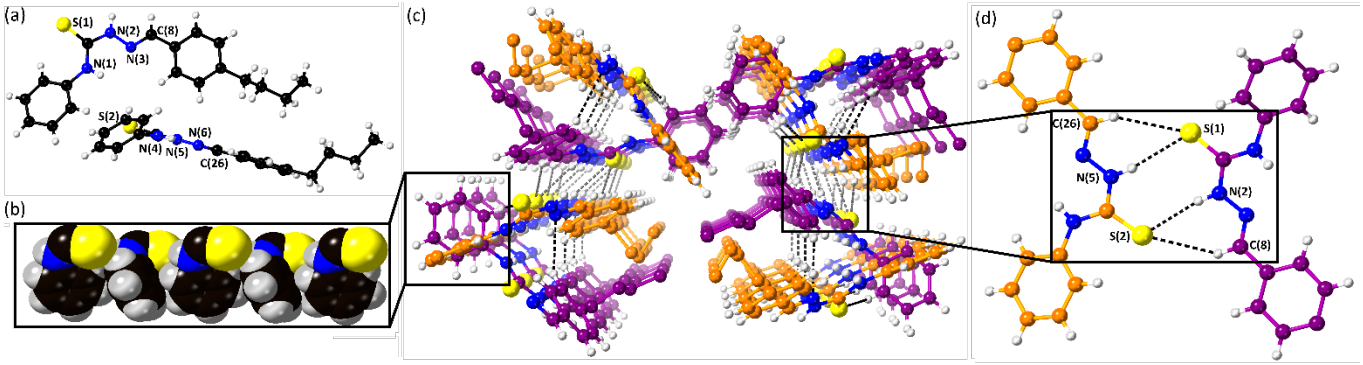

Fig. 2. (a) Two crystallographically unique receptors **1** found in the asymmetric unit. (b) phenyl ring edge-to-face stacking observed between both crystallographically unique receptors. (c) Packing diagram of **1** shown along the *a* axis with carbon atoms from each receptor coloured either purple or orange for clarity. Black dashed bonds represent close H bonds holding together a pair of receptors while grey dashed bonds represent close H bonds between the pairs. Hydrogen atoms on butyl chains omitted for clarity. (d) Hydrogen bonding $R_2^2(6)$ and $R_2^2(8)$ motifs between receptor pairs.

3.2 pH-dependent Cl^-/NO_3^- exchange studies

The transporters were initially evaluated for their pH switchability by comparing their Cl^-/NO_3^- exchange activities under neutral and acidic conditions. POPC vesicles with internal NaCl (489 mM) buffered at pH 4.5 or 7.2 were suspended in a $NaNO_3$ (489 mM) external solution buffered at pH 4.5 or 7.2. Anion transporters were added to the vesicles as DMSO solutions and Cl^- efflux facilitated by an anion transporter was monitored using a chloride ion selective electrode (ISE). Similarly to previously reported PTSCs, transporters **1**–**9** were inactive Cl^-/NO_3^- exchangers at pH 7.2 but became "switched ON" to facilitate rapid anion exchange at pH 4.5 (Figs. 3, S20–S37). To quantify the pH switchability, concentration-dependent Hill plot analysis were conducted to give an effective transporter concentration that facilitates 50% of Cl^- efflux at 270 s (EC_{50} values) at pH 4.5 and pH 7.2.

As shown by Table 1, compound **1** was identified as the most active anion transporter, showing a low EC_{50} of 0.0175 mol% (with respect to lipids) at pH 4.5 and ~550-fold reduced activity at pH 7.0. For transporters **5** and **7**–**9**, the Cl^-/NO_3^- exchange was almost completely suppressed at pH 7.2, with modest-to-high activities observed at pH 4.5. The much weaker anion transport activities of **5** and **7**–**9** at pH 7.2 compared with **1**–**3** are attributed to the presence of electron-withdrawing substituents lowing the pK_a of the iminium group and thereby inhibiting imine protonation at pH 7.2 as required for anion transport. Transporter **6** precipitated upon addition to the vesicle suspensions as DMSO solutions which prohibited a detailed analysis of its pH switchability.

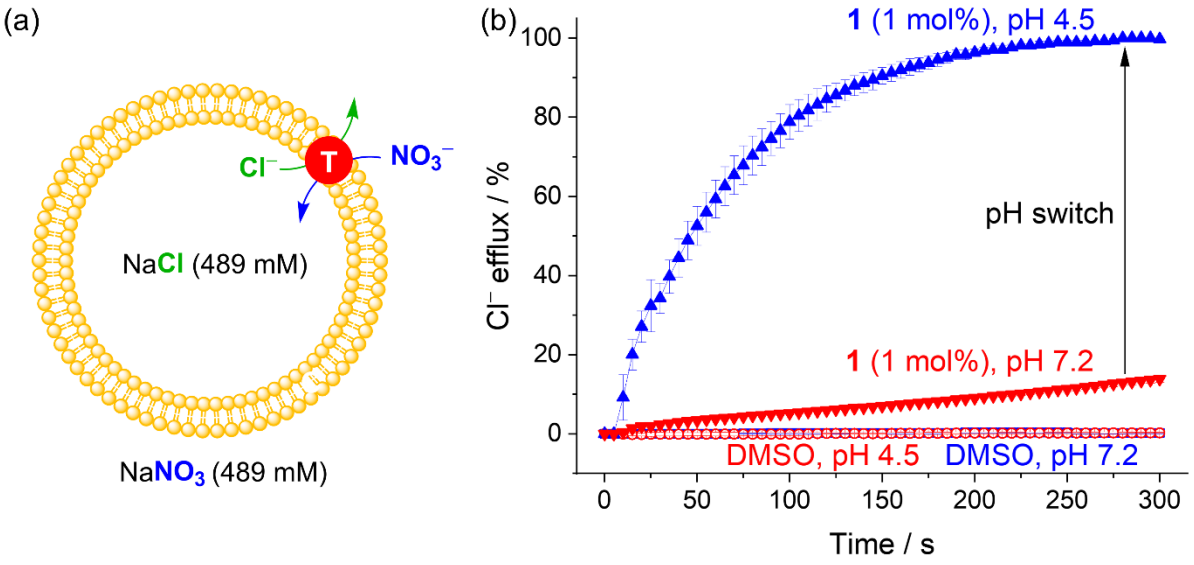

Fig. 3. (a) Schematic representation of the Cl^-/NO_3^- exchange assay. (b) Cl^-/NO_3^- exchange assay for transporter **1** and DMSO control using vesicles with internal and external solutions buffered at pH 4.5 (blue) and pH 7.2 (red). Error bars represent standard deviations from three runs.

Table 1 Hill analysis for Cl^-/NO_3^- exchange by PTSCs **1** – **9**.

PTSC	Cl^-/NO_3^- at pH 7.2		Cl^-/NO_3^- at pH 4.5		EC_{50} (pH 7.2) / EC_{50} (pH 4.5)
	EC_{50} / mol%	*n*	EC_{50} / mol%	*n*	
1	9.6	1.2	0.018	1.7	550
2	3.9	0.92	0.020	1.8	190
3	2.8	1.6	0.044	0.82	64
4	–[a]	–[a]	8.5	0.35	–[a]
5	–[a]	–[a]	0.17	0.44	–[a]
6	–[a]	–[a]	–[a]	–[a]	–[a]
7	–[a]	–[a]	0.035	1.0	–[a]
8	–[a]	–[a]	3.7	0.36	–[a]
9	–[a]	–[a]	1.1	0.66	–[a]

[a] Too inactive for Hill analysis.

3.3 pH-dependent studies of Cl^- uniport and H^+/Cl^- symport

With the pH-dependent Cl^-/NO_3^- exchange confirmed for the new PTSCs, we next investigated the Cl^- uniport and H^+/Cl^- symport activities of transporters **1**–**9** at pH 4.5 and pH 7.2 using our previously developed cationophore-coupled ISE assays.[15] These assays complement the Cl^-/NO_3^- exchange assay by providing additional insights into electrogenic/electroneutral transport phenomena and revealing the potentially slow NO_3^- transport that could rate-limit the Cl^-/NO_3^- exchange process.[16] POPC vesicles were loaded with KCl (300 mM) at pH 4.5 or 7.2, and suspended in an external solution containing inert K_2SO_4 (150 mM) at pH 4.5 or 7.2. Anion transporters were added along with a cationophore (valinomycin or monensin) to facilitate KCl efflux. In the presence of K^+ uniporter valinomycin, the anion transporter needs to facilitate Cl^- uniport to give KCl efflux (Fig. 4a bottom). By contrast, in the presence of K^+/H^+ exchanger monensin, H^+/Cl^- symport facilitated by the anion transporter is required to generate net KCl efflux (Fig. 4a top). Similar to prodigiosin, the previously reported PTSCs were shown to facilitate H^+/Cl^- symport (coupling to monensin) but no Cl^- uniport (coupling to valinomycin) at pH 4.5.[11] This was attributed to the inability of the cationic protonated $PTSCH^+$ (decomplexed transporter) to diffuse through the membrane without a bound anion. Back diffusion of the decomplexed transporter is a necessary step for Cl^- uniport but not for anion exchange or H^+/Cl^- symport.[17] Previously, the cationophore-coupled assays were not conducted at pH 7.2.

Consistent with previous findings, the new PTSCs **1**–**9** induced efficient Cl^- efflux with monensin and low-to-negligible Cl^- efflux with valinomycin at pH 4.5 (Fig. 4 blue, Table 2), indicating the strong preference for H^+/Cl^- symport over Cl^- uniport for these transporters. Significant Cl^- uniport activities (relative to H^+/Cl^- symport activities), however, could be observed for polyfluorinated transporters **6**, **8** and **9** at pH 7.2. This can be attributed to the neutral form of PTSCs facilitating Cl^- uniport *via* Cl^- binding in the *syn*-conformation (Fig. 1a left) followed by transmembrane diffusion of the anionic complex, release of Cl^- and the back diffusion of the neutral uncomplexed PTSC. This alternative mechanism required a significant anion binding affinity of the neutral form (in which only one thiourea NH and a weak imine CH donor are available for anion binding) and therefore was only observed for the more acidic transporters in the series.

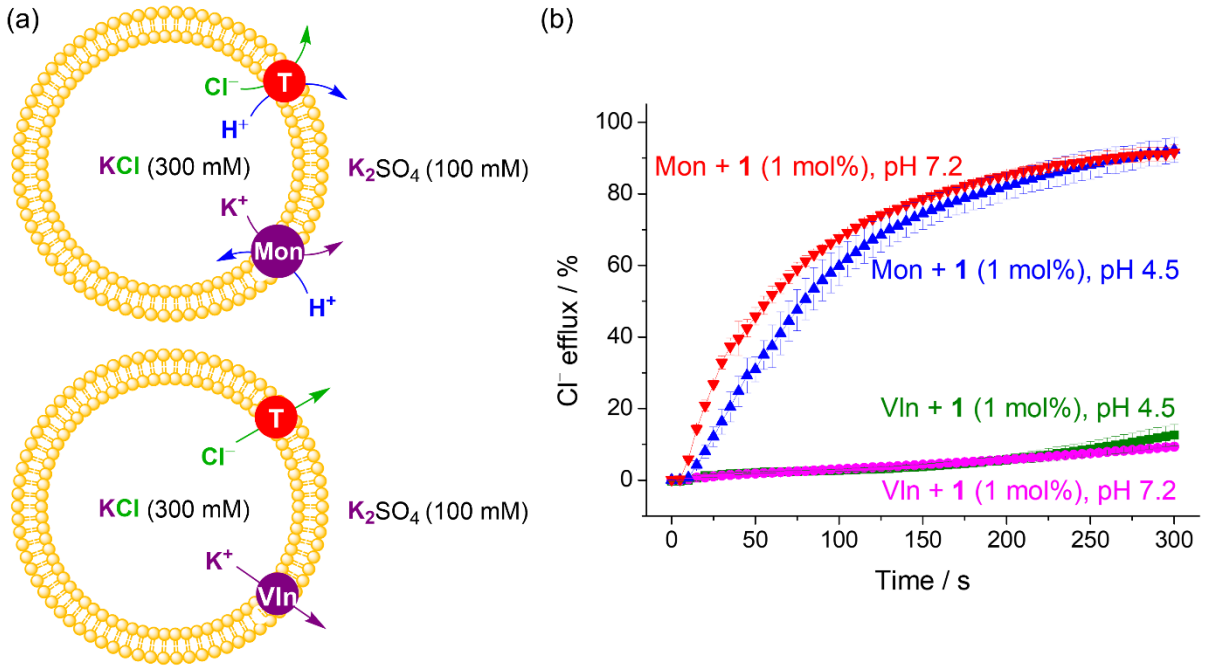

Fig. 4. (a) Schematic representation of H^+/Cl^- symport (top, anion transporter T coupling to monensin, Mon) and Cl^- uniport (bottom, anion transporter T coupling to valinomycin, Vln) assays. (b) H^+/Cl^- symport (red and blue) and Cl^- uniport (green and pink) assays for transporter **1** at pH 4.5 (blue and green) and pH 7.2 (red and pink). The Cl^- efflux induced by the anion transporter or cationophore alone is negligible (Fig. S38). Error bars represent standard deviations from three runs.

Table 2 Cationophore-coupled assays for PTSCs **1**–**9**.

PTSC	Concentration	pH 7.2		pH 4.5	
		Cl^- efflux at 300 s / %		Cl^- efflux at 300 s / %	
		Mon[a]	Vln[b]	Mon[a]	Vln[b]
1	1 mol%	92	9.4	92	13
2	1 mol%	100	15	81	8.3
3	1 mol%	99	6.2	83	6.2
4	10 mol%	49	13	33	7.5
5	10 mol%	50	8.3	38	3.4
6	10 mol%	9.4	8.4	3.9	0.60
7	1 mol%	95	19	98	11
8	10 mol%	35	15	12	3.3
9	10 mol%	49	28	20	5.5

[a] Cl^- efflux by PTSC in the presence of monensin (Mon, 0.1 mol%), which indicates the H^+/Cl^- symport activity of PTSC.

[b] Cl^- efflux by PTSC in the presence of valinomycin (Vln, 0.1 mol%), which indicates the Cl^- uniport activity of PTSC.

Surprisingly, while these PTSCs are inactive Cl^-/NO_3^- exchangers at pH 7.2, we observed highly efficient H^+/Cl^- symport (coupling to monensin) for all compounds at pH 7.2 (Fig. 4b red, Table 2). No enhancement of H^+/Cl^- symport activity was observed on acidifying the vesicle suspensions from 7.2 to 4.5. These results appear to indicate the lack of pH switchability for the H^+/Cl^- symport facilitated by PTSCs in the tested pH range, contrasting the strong pH switchability in the Cl^-/NO_3^- exchange assay (Fig. 3, Table 1).

We hypothesised that the seemingly contradictory pH-dependent results in the two assays could be related to different rate-limiting steps for H^+/Cl^- symport and Cl^-/NO_3^- exchange. As shown by our previous studies, most hydrogen bond-based anion transporters facilitate the transport of the more lipophilic anion NO_3^- faster than Cl^- as governed by the ease of anion dehydration. However, exceptions have been found for a few transporters, most notably the tripodal tris-(thio)ureas [16, 18]. These transporters are $Cl^- > NO_3^-$ selective due to their structural mismatch for binding planar NO_3^- ions, leading to underestimated Cl^- transport activity when tested under the Cl^-/NO_3^- exchange assay.

3.3 Anion transport selectivity studies

To understand the pH-dependent Cl^-/NO_3^- exchange property of the PTSCs, we determined the anion transport selectivity of **1** as a representative example under an HPTS assay utilising a transmembrane anion gradient to induce a pH gradient (Fig. 5a).[19] In this assay, vesicles containing NaCl (100 mM) and the pH indicator HPTS (1 mM) buffered at pH 7.0 were suspended in NaX (100 mM, X = Cl^-, Br^-, NO_3^-, I^-, or ClO_4^-) at pH 7.0. Transporter **1** was added to induce a pH gradient where an acidification of the vesicular interiors indicates faster HX influx than HCl efflux (i.e., $X^- > Cl^-$ selectivity) and *vice versa*. The assay revealed a selectivity pattern of $I^- > Br^- > Cl^- > ClO_4^- > NO_3^-$ (Fig. 5b). Compared with a neutral mono-thiourea transporter showing a Hofmeister-type selectivity pattern (i.e., $ClO_4^- > I^- > NO_3^- > Br^- > Cl^-$),[19] the selectivity profile of **1** features a strong halide-over-oxyanion preference with the selectivity sequence within each category (halides or oxyanions) governed by the ease of anion dehydration. This halide selectivity presumably originated from the covalent character of the strong doubly ionic hydrogen bonds[20] in anion binding by protonated PTSCs. As the lone pair orbitals (HOMOs) of the halide ions are of higher energies than those of the tested oxyanions (ClO_4^- and NO_3^-), charge transfer between the anion HOMO and the antibonding orbital (LUMO) of the hydrogen bond donor is more favourable for halides than for the oxyanions, which accounts for the halide over oxyanion selectivity here observed for doubly ionic hydrogen bonds. Corroborating the abovementioned hypothesis, a similar halide over oxyanion selectivity has been observed with a Pd(II)-based anion transporter in which anion binding (via metal coordination) features a strong covalent character.[21] Unfortunately, we were unable to determine the anion binding constants for the protonated PTSCs to evaluate the anion binding selectivity because of their instability.[11] To quantify the Cl^- vs NO_3^- transport selectivity of **1**, a pH gradient dissipation assay[22] was conducted by applying a transmembrane pH gradient (pH 7.0 inside and pH 8.0) and measuring the rate of pH gradient dissipation under $NaCl^{in}/NaCl^{out}$ and $NaNO_3^{in}/NaNO_3^{out}$ conditions. These assays have been designed to evaluate H^+/X^- symport activities of anion transporters (Fig. 5b). The results demonstrate rapid H^+/Cl^- symport and no discernible H^+/NO_3^- symport from DMSO control baseline for transporter **1** used at the same concentration (Fig. 5d), confirming its extremely high $Cl^- > NO_3^-$ selectivity at neutral to slightly basic pH.

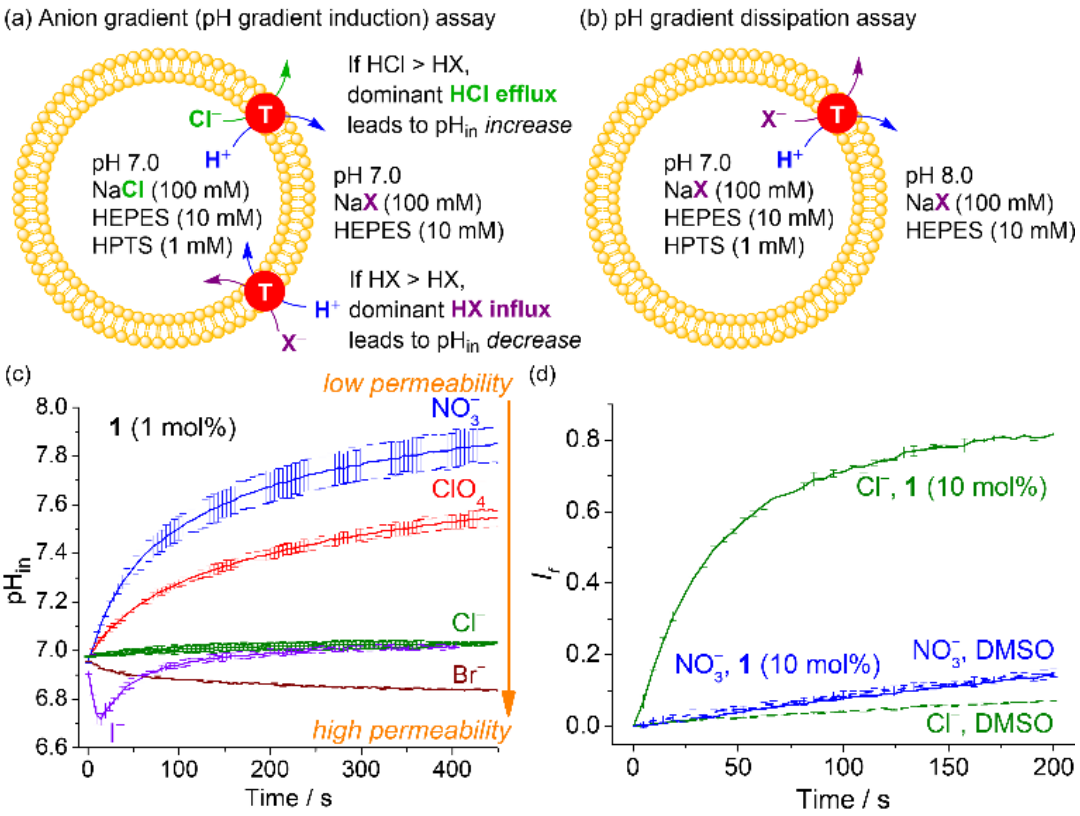

Fig. 3. Determination of anion transport selectivity of **1** using an anion gradient (pH gradient induction) assay (a, c) and a pH gradient dissipation assay (b, d). In (c) purple line, efficient Cl^-/I^- exchange led to rapid dissipation of the initially induced pH gradient. Note that in (d) **1** was tested at a higher concentration because of the lowered transporter activity under the assay conditions (pH 8.0 outside). Error bars represent standard deviations from two runs.

The abovementioned selectivity results indicate the rate-limiting NO_3^- transport process as the determinant for the pH switchable Cl^-/NO_3^- exchange by PTSCs. In lipid-water biphasic systems, NO_3^- binding to the protonated PTSCs is expected to be drastically weaker than Cl^- binding. As a result, a lower solution pH is required to shift the equilibrium from the free neutral PTSC to the $PTSCH^+\cdots X^-$ ion pair complex for NO_3^- binding than for Cl^- binding. This leads to inhibition of the Cl^-/NO_3^- exchange by slow NO_3^- transport at pH 7.2 and the "switch-ON" of the Cl^-/NO_3^- exchange by enhanced NO_3^- binding equilibrium at pH 4.5. In addition, at neutral pH under the $NaCl^{in}/NaNO_3^{out}$ ISE assay conditions, the vesicle interiors were basified due to selective HCl efflux by PTSCs (Fig. 5c blue), which could further reduce the ability of the PTSCs to form protonated anion complexes.

4. Conclusions

In summary, we have developed an expanded class of phenylthiosemicarbazones as pH-switchable Cl^-/NO_3^- exchangers with supressed activity at pH 7.2 and enhanced activity at pH 4.5. We showed that these transporters are active H^+/Cl^- symporters and inactive Cl^- uniporters at pH 4.5 similar to the behaviour of prodigiosin. Most importantly, we demonstrate the strong halide over oxyanion transport selectivity of the phenylthiosemicarbazones presumably due to the covalency of the doubly ionic hydrogen bond interactions leading to the preference for halide ions over oxyanions with low HOMO energies. As a result, while Cl^- transport was efficient at both pH 4.5 and pH 7.2, the slow NO_3^- transport turned out to be the rate-limiting factor for the suppressed Cl^-/NO_3^- exchange at pH 7.2 and the activation at pH 4.5. Our results provide important insights for understanding the

behaviour and improving the robustness of pH-dependent anion transporters aimed at therapeutic applications. In particular, the study demonstrates the limitation of the anion exchange assay and the benefit of measuring pH-dependent H^+/Cl^- symport and Cl^- uniport activities when studying pH-switchable transporters.

Acknowledgements

We acknowledge and pay respect to the Gadigal people of the Eora Nation, the traditional owners of the land on which we research, teach and collaborate at the University of Sydney. P.A.G. thanks the University of Sydney and the Australian Research Council (DP200100453) for funding.

References

[1] J.T. Davis, P.A. Gale, R. Quesada, Advances in anion transport and supramolecular medicinal chemistry, Chem. Soc. Rev., 49 (2020) 6056-6086.
[2] X. Wu, A.M. Gilchrist, P.A. Gale, Prospects and Challenges in Anion Recognition and Transport, Chem, 6 (2020) 1296-1309.
[3] T. Sato, H. Konno, Y. Tanaka, T. Kataoka, K. Nagai, H.H. Wasserman, S. Ohkuma, Prodigiosins as a new group of H^+/Cl^- symporters that uncouple proton translocators, J. Biol. Chem., 273 (1998) 21455-21462.
[4] S. Ohkuma, T. Sato, M. Okamoto, H. Matsuya, K. Arai, T. Kataoka, K. Nagai, H.H. Wasserman, Prodigiosins uncouple lysosomal vacuolar-type ATPase through promotion of H^+/Cl^- symport, Biochem. J., 334 (1998) 731-741.
[5] T. Kataoka, M. Muroi, S. Ohkuma, T. Waritani, J. Magae, A. Takatsuki, S. Kondo, M. Yamasaki, K. Nagai, Prodigiosin 25-C uncouples vacuolar type H^+-ATPase, inhibits vacuolar acidification and affects glycoprotein processing, FEBS Lett., 359 (1995) 53-59.
[6] Z.-K. Wang, X.-Q. Hong, J. Hu, Y.-Y. Xing, W.-H. Chen, Synthesis and biological activity of squaramido-tethered bisbenzimidazoles as synthetic anion transporters, RSC Adv., 11 (2021) 3972-3980.
[7] L. Tapia, Y. Pérez, M. Bolte, J. Casas, J. Solà, R. Quesada, I. Alfonso, pH-Dependent Chloride Transport by Pseudopeptidic Cages for the Selective Killing of Cancer Cells in Acidic Microenvironments, Angew. Chem. Int. Ed., 58 (2019) 12465-12468.
[8] A. Saha, N. Akhtar, V. Kumar, S. Kumar, H.K. Srivastava, S. Kumar, D. Manna, pH-Regulated anion transport activities of bis(iminourea) derivatives across the cell and vesicle membrane, Org. Biomol. Chem., 17 (2019) 5779-5788.
[9] A. Roy, D. Saha, P.S. Mandal, A. Mukherjee, P. Talukdar, pH-Gated Chloride Transport by a Triazine-Based Tripodal Semicage, Chem. Eur. J., 23 (2017) 1241-1247.
[10] N. Busschaert, R.B.P. Elmes, D.D. Czech, X. Wu, I.L. Kirby, E.M. Peck, K.D. Hendzel, S.K. Shaw, B. Chan, B.D. Smith, K.A. Jolliffe, P.A. Gale, Thiosquaramides: pH switchable anion transporters, Chem. Sci., 5 (2014) 3617-3626.
[11] E.N.W. Howe, N. Busschaert, X. Wu, S.N. Berry, J. Ho, M.E. Light, D.D. Czech, H.A. Klein, J.A. Kitchen, P.A. Gale, pH-Regulated Nonelectrogenic Anion Transport by Phenylthiosemicarbazones, J. Am. Chem. Soc., 138 (2016) 8301-8308.
[12] G. Sheldrick, A short history of SHELX, Acta Crystallogr. A, 64 (2008) 112-122.
[13] G. Sheldrick, Crystal structure refinement with SHELXL, Acta Crystallogr. C, 71 (2015) 3-8.
[14] O.V. Dolomanov, L.J. Bourhis, R.J. Gildea, J.A.K. Howard, H. Puschmann, OLEX2: a complete structure solution, refinement and analysis program, J. Appl. Crystallogr., 42 (2009) 339-341.
[15] X. Wu, E.N.W. Howe, P.A. Gale, Supramolecular Transmembrane Anion Transport: New Assays and Insights, Acc. Chem. Res., 51 (2018) 1870-1879.
[16] Y. Yang, X. Wu, N. Busschaert, H. Furuta, P.A. Gale, Dissecting the chloride-nitrate anion transport assay, Chem. Commun., 53 (2017) 9230-9233.

[17] X. Wu, J.R. Small, A. Cataldo, A.M. Withecombe, P. Turner, P.A. Gale, Voltage-Switchable HCl Transport Enabled by Lipid Headgroup–Transporter Interactions, Angew. Chem. Int. Ed., 58 (2019) 15142-15147.
[18] L.A. Jowett, E.N.W. Howe, X. Wu, N. Busschaert, P.A. Gale, New Insights into the Anion Transport Selectivity and Mechanism of Tren-based Tris-(thio)ureas, Chem. Eur. J., 24 (2018) 10475-10487.
[19] X. Wu, P.A. Gale, Measuring anion transport selectivity: a cautionary tale, Chem. Commun., 57 (2021) 3979-3982.
[20] P.A. Hunt, C.R. Ashworth, R.P. Matthews, Hydrogen bonding in ionic liquids, Chem. Soc. Rev., 44 (2015) 1257-1288.
[21] D. Milano, B. Benedetti, M. Boccalon, A. Brugnara, E. Iengo, P. Tecilla, Anion transport across phospholipid membranes mediated by a diphosphine-Pd(II) complex, Chem. Commun., 50 (2014) 9157-9160.
[22] S. Matile, N. Sakai, The characterization of synthetic ion channels and pores, in: C.A. Schalley (Ed.) Analytical Methods in Supramolecular Chemistry, Wiley-VCH, Place Published, 2012, pp. 711-742.

Supplementary Material

Halide-selective, proton-coupled anion transport by phenylthiosemicarbazones

Ethan N.W. Howe,[a] Vai-Vai Tiffany Chang,[a] Xin Wu,[a] William Lewis,[a] Lauren K. Macreadie,[a] and Philip A. Gale *[a,b]

[a] *School of Chemistry, The University of Sydney, NSW 2006, Australia*

[b] *The University of Sydney Nano Institute (SydneyNano), The University of Sydney, NSW 2006, Australia*

*Corresponding author. Email: philip.gale@sydney.edu.au

Contents

S1 Compound characterisations

Characterisation of (*E*)-2-(4-butylbenzylidene)-*N*-phenylhydrazine-1-carbothioamide 1

Afforded white crystalline solid (94% yield), mp 162-163 °C.

^{1}H NMR (400 MHz, $(CD_3)_2SO$, 298 K, ppm) δ: 11.77 (s, 1H, N*H*$^{\beta}$), 10.06 (s, 1H, N*H*$^{\alpha}$), 8.13 (s, 1H, NC*H*), 7.80 (d, *J* = 8.3 Hz, 2H, Ar*H* × 2), 7.57 (d, *J* = 8.0 Hz, 2H, Ar*H* × 2), 7.37 (t, *J* = 7.6 Hz, 2H, Ar*H* × 2), 7.25 (d, *J* = 8.0 Hz, 2H, Ar*H* × 2), 7.20 (t, *J* = 7.3 Hz, 1H, Ar*H*), 2.61 (t, *J* = 7.7 Hz, 2H, CH_2), 1.56 (quint, *J* = 7.9 Hz, 2H, CH_2), 1.31 (sext, *J* = 7.5 Hz, 2H, CH_2), 0.90 (t, *J* = 7.2 Hz, 3H, CH_3).

^{13}C NMR (101 MHz, $(CD_3)_2SO$, 298 K, ppm) δ: 144.7, 143.0, 139.1, 131.5, 128.6, 128.0, 127.6, 125.8, 125.2, 34.7, 32.9, 21.7, 13.7.

MS (APCI^{+}) m/z: calcd for $C_{18}H_{22}N_3S$: 312.15, found: 312.09.

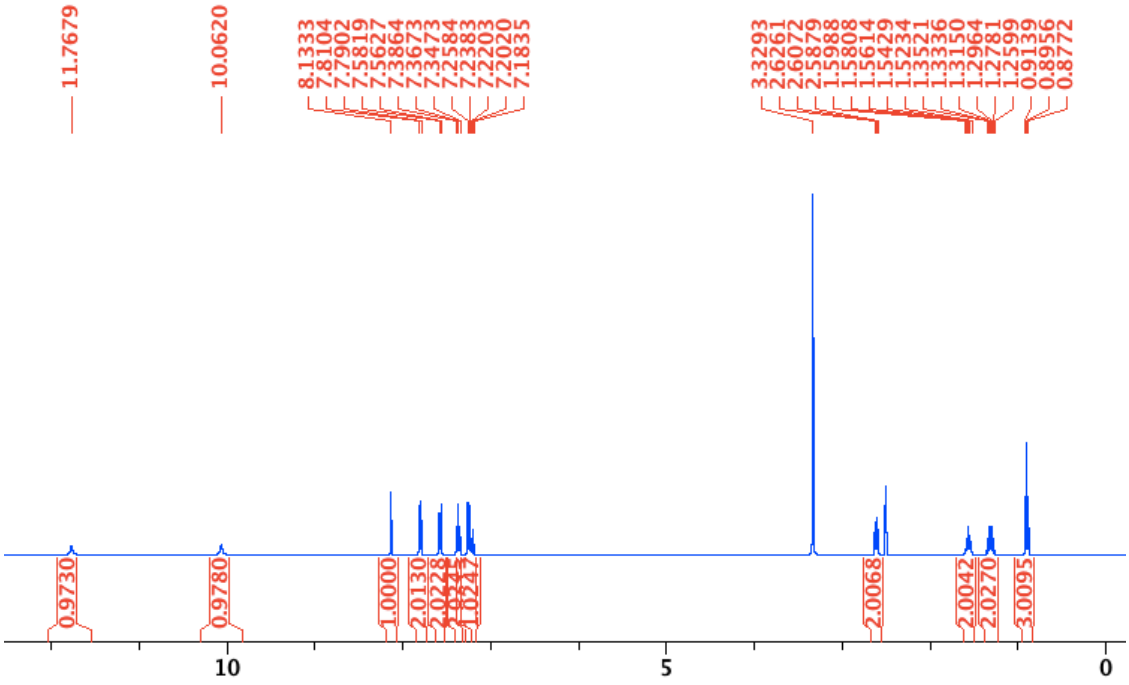

Fig. S1 ^{1}H NMR (400 MHz) spectrum of compound **1** in DMSO-d_6.

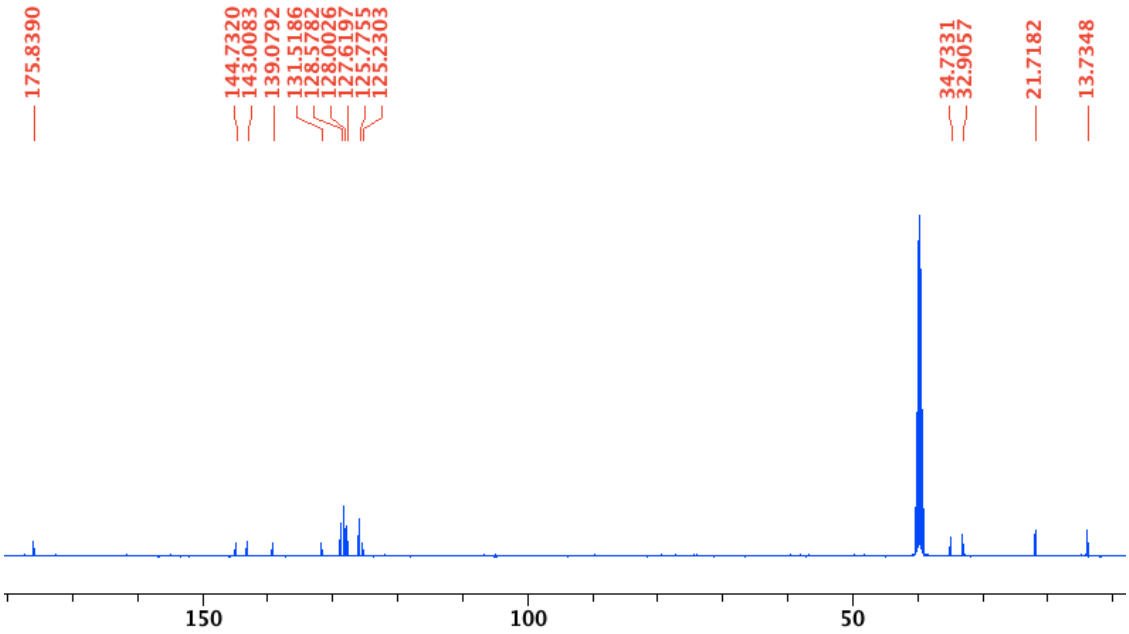

Fig. S2 ^{13}C NMR (101 MHz) spectrum of compound **1** in DMSO-*d*$_6$.

Characterisation of (*E*)-2-(4-butylbenzylidene)-*N*-(*p*-tolyl)hydrazine-1-carbothioamide 2

Afforded white crystalline solid (96% yield), mp 152-153 °C

^{1}H NMR (400 MHz, $(CD_3)_2SO$, 298 K, ppm) δ: 11.72 (s, 1H, N*H*$^{\beta}$), 9.99 (s, 1H, N*H*$^{\alpha}$), 8.12 (s, 1H, NC*H*), 7.79 (d, *J* = 8.5 Hz, 2H, Ar*H* × 2), 7.43 (d, *J* = 8.5 Hz, 2H, Ar*H* × 2), 7.24 (d, *J* = 8.1 Hz, 2H, Ar*H* × 2), 7.17 (d, *J* = 8.5 Hz, 2H, Ar*H* × 2), 2.60 (t, *J* = 7.6 Hz, 2H, C*H*$_2$), 2.31 (s, 3H, C*H*$_3$), 1.56 (quint, *J* = 7.8 Hz, 2H, C*H*$_2$), 1.31 (sext, *J* = 7.4 Hz, 2H, C*H*$_2$), 0.89 (t, *J* = 7.4 Hz, 3H, C*H*$_3$).

^{13}C NMR (101 MHz, $(CD_3)_2SO$, 298 K, ppm) δ: 175.9, 144.7, 142.8, 136.5, 134.4, 131.6, 128.6, 128.5, 127.6, 125.7, 34.7, 32.9, 21.7, 20.6, 13.7.

MS (APCI$^+$) m/z: calcd for $C_{19}H_{24}N_3S$: 326.17, found: 326.13.

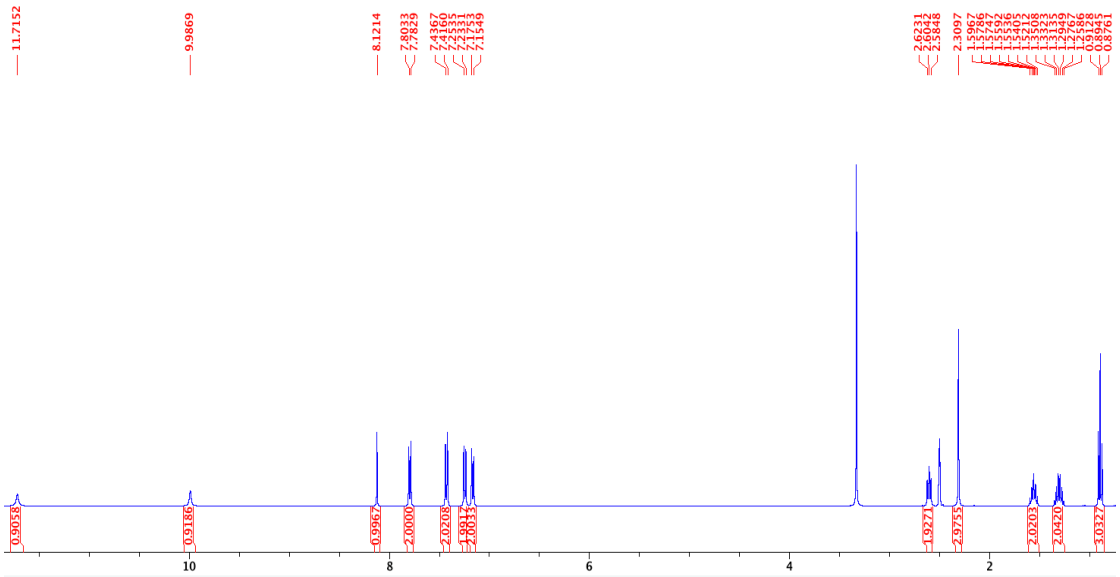

Fig. S3 ^{1}H NMR (400 MHz) spectrum of compound **2** in DMSO-*d*$_6$.

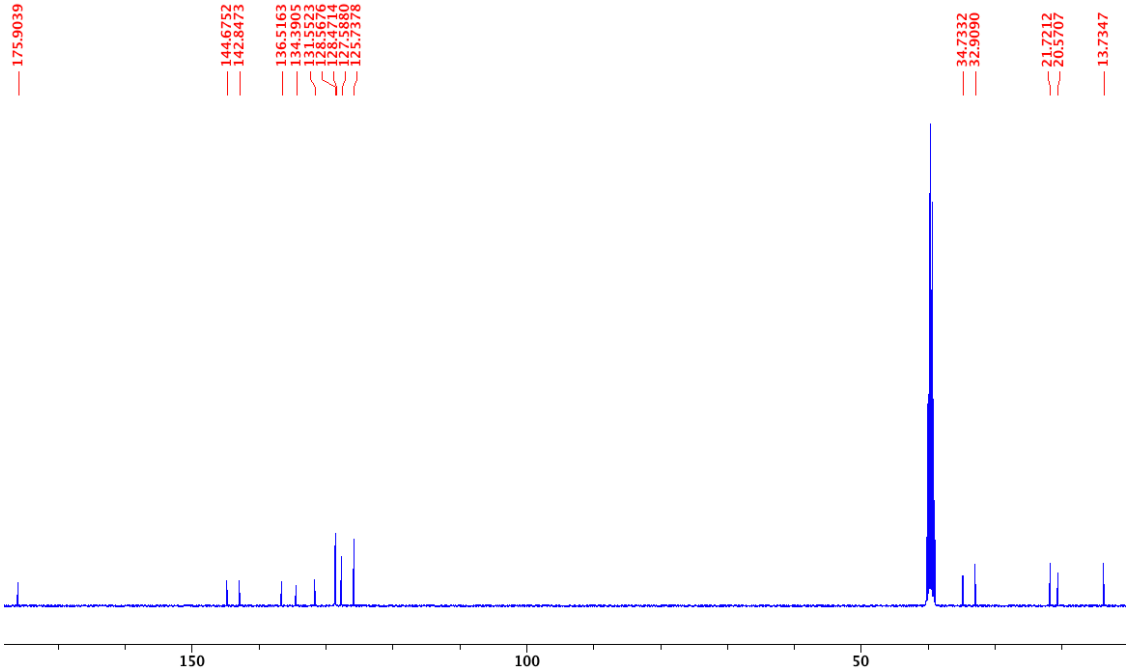

Fig. S4 ^{13}C NMR (101 MHz) spectrum of compound **2** in DMSO-*d*$_6$.

Characterisation of (*E*)-2-(4-butylbenzylidene)-*N*-(4-methoxyphenyl)hydrazine-1-carbothioamide 3

Afforded white solid (90% yield), mp 126-128 °C

^{1}H NMR (400 MHz, $(CD_3)_2SO$, 298 K, ppm) δ: 11.68 (s, 1H, N*H*$^{\beta}$), 9.96 (s, 1H, N*H*$^{\alpha}$), 8.11 (s, 1H, NC*H*), 7.79 (d, *J* = 7.9 Hz, 2H, Ar*H* × 2), 7.40 (d, *J* = 8.7 Hz, 2H, Ar*H* × 2), 7.24 (d, *J* = 8.3 Hz, 2H, Ar*H* × 2), 6.93 (d, *J* = 9.1 Hz, 2H, Ar*H* × 2), 3.77 (s, 3H, OCH_3), 2.60 (t, *J* = 7.5 Hz, 2H, CH_2), 1.56 (quint, *J* = 7.6 Hz, 2H, CH_2), 1.31 (sext, *J* = 7.5 Hz, 2H, CH_2), 0.89 (t, *J* = 7.3 Hz, 3H, CH_3).

^{13}C NMR (101 MHz, $(CD_3)_2SO$, 298 K, ppm) δ: 176.2, 156.9, 144.6, 142.7, 132.0, 131.6, 128.6, 127.6, 127.5, 113.2, 55.2, 34.7, 32.9, 21.7, 13.7.

MS (APCI$^+$) m/z: calcd for $C_{19}H_{24}N_3OS$: 342.16, found: 342.12.

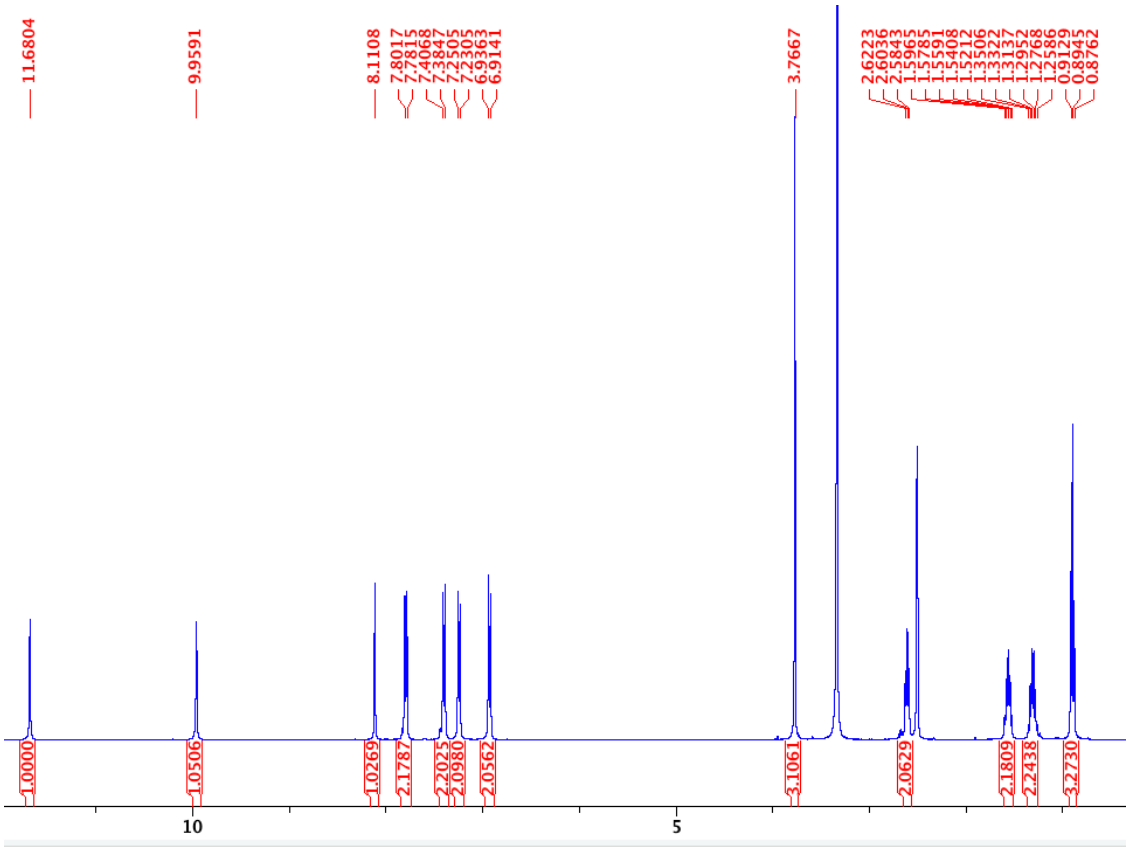

Fig. S5 ^{1}H NMR (400 MHz) spectrum of compound **3** in DMSO-*d*$_6$.

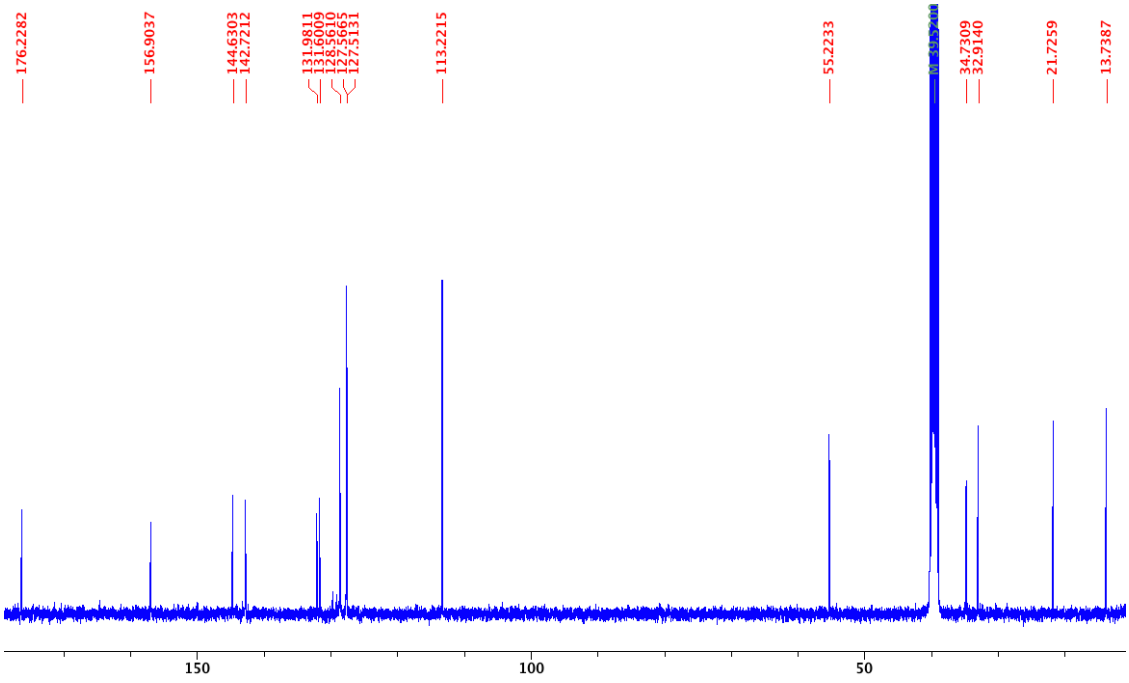

Fig. S6 ^{13}C NMR (101 MHz) spectrum of compound **3** in DMSO-*d*$_6$.

Characterisation of (*E*)-2-(4-butylbenzylidene)-*N*-(4-(trifluoromethyl)phenyl)hydrazine-1-carbothioamide 4

Afforded white crystalline solid (95% yield), mp 167-169 °C

^{1}H NMR (400 MHz, $(CD_3)_2SO$, 298 K, ppm) δ: 11.98 (s, 1H, N*H*$^{\beta}$), 10.26 (s, 1H, N*H*$^{\alpha}$), 8.17 (s, 1H, NC*H*), 7.91 (d, *J* = 8.4 Hz, 2H, Ar*H* × 2), 7.81 (d, *J* = 8.0 Hz, 2H, Ar*H* × 2), 7.73 (d, *J* = 8.7 Hz, 2H, Ar*H* × 2), 7.26 (d, *J* = 8.0 Hz, 2H, Ar*H* × 2), 2.61 (t, *J* = 7.6 Hz, 2H, CH_2), 1.56 (quint, *J* = 7.6 Hz, 2H, CH_2), 1.31 (sext, *J* = 7.5 Hz, 2H, CH_2), 0.89 (t, *J* = 7.5 Hz, 3H, CH_3).

^{13}C NMR (101 MHz, $(CD_3)_2SO$, 298 K, ppm) δ: 175.6, 145.0, 143.8, 142.8, 131.3, 128.6, 127.7, 125.4, 125.1 (q, ^{3}J(C,F) = 4 Hz), 125.0 (q, ^{2}J(C,F) = 32 Hz), 124.3 (q, ^{1}J(C,F) = 272 Hz), 34.7, 32.9, 21.7, 13.7.

^{19}F NMR (376 MHz, DMSO-d6, dppm) δ: -60.47 (s, 3F)

MS (APCI^{+}) m/z: calcd for $C_{19}H_{21}F_3N_3S$: 380.14, found: 380.10.

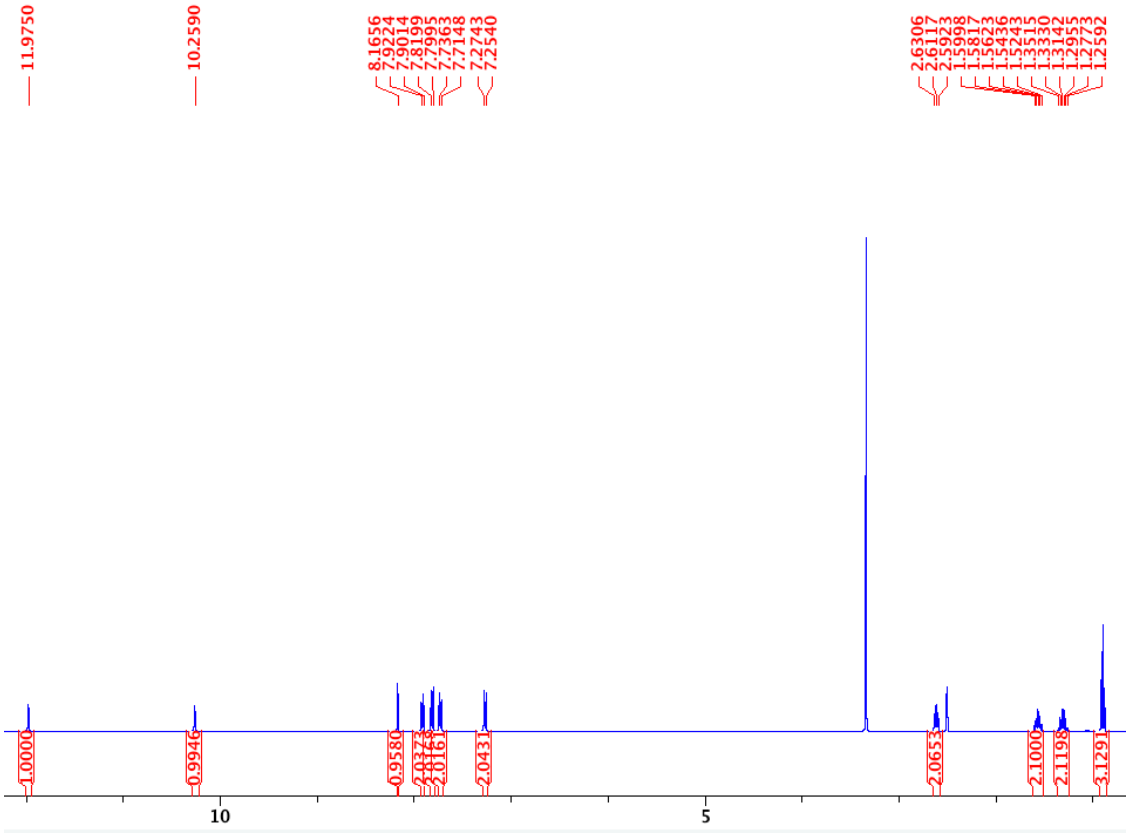

Fig. S7 ^{1}H NMR (400 MHz) spectrum of compound **4** in DMSO-d_6.

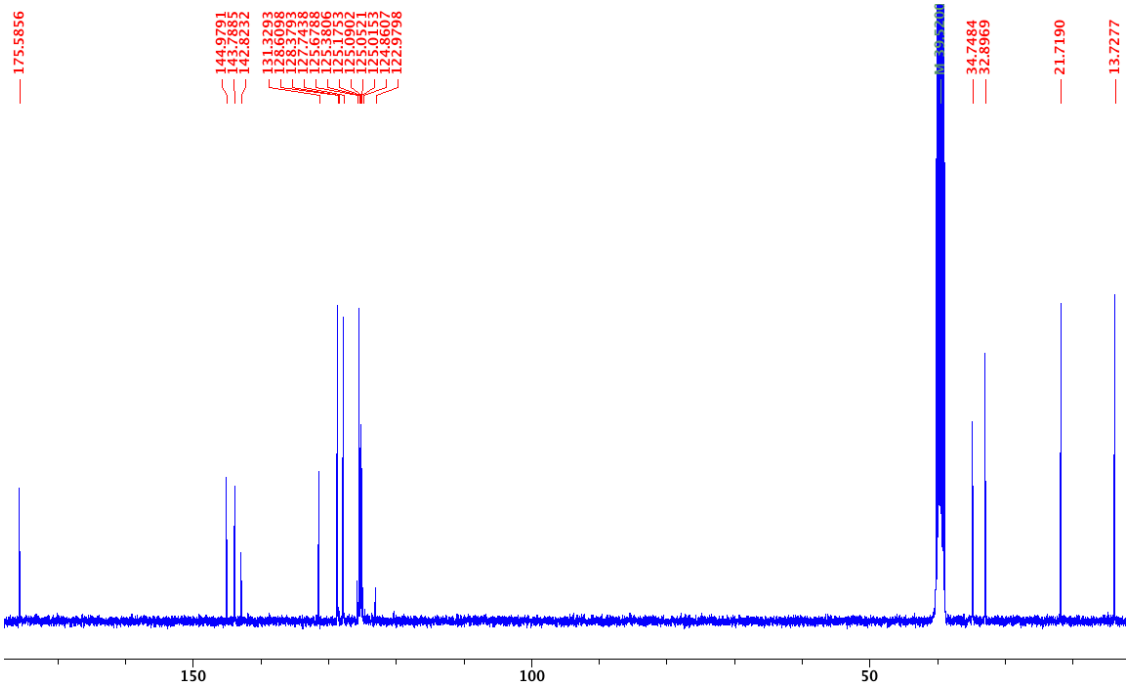

Fig. S8 ^{13}C NMR (101 MHz) spectrum of compound **4** in DMSO-d_6.

Characterisation of (*E*)-2-(4-butylbenzylidene)-*N*-(4-(trifluoromethoxy)phenyl)hydrazine-1-carbothioamide 5

Afforded white solid (91% yield), mp 122-125 °C

^{1}H NMR (400 MHz, $(CD_3)_2SO$, 298 K, ppm) δ: 11.16 (s, 1H, N*H*$^{\beta}$), 10.42 (s, 1H, N*H*$^{\alpha}$), 8.69 (s, 1H, NC*H*), 8.35 (d, *J* = 8.9 Hz, 2H, Ar*H* × 2), 8.21 (d, *J* = 8.0 Hz, 2H, Ar*H* × 2), 7.77 (d, *J* = 8.9 Hz, 2H, Ar*H* × 2), 7.73 (d, *J* = 8.0 Hz, 2H, Ar*H* × 2), 3.11 (t, *J* = 7.6 Hz, 2H, CH_2), 2.06 (quint, *J* = 7.6 Hz, 2H, CH_2), 1.81 (sext, *J* = 7.4 Hz, 2H, CH_2), 1.37 (t, *J* = 7.5 Hz, 3H, CH_3).

^{13}C NMR (101 MHz, $(CD_3)_2SO$, 298 K, ppm) δ: 187.2, 156.4 (d, ^{3}J(C,F) = 2 Hz), 156.1, 153.9, 148.9, 142.2, 139.4, 138.2, 136.7 (d, ^{2}J(C,F) = 26 Hz), 136.7, 131.4, 131.2 (d, ^{1}J(C,F) = 255 Hz), 45.8, 43.9, 32.6, 23.8.

^{19}F NMR (376 MHz, DMSO-d6, dppm) δ: -58.68 (s, 3F)

MS (ESI^{+}) m/z: calcd for $C_{19}H_{21}F_3N_3OS$: 396.14, found: 396.17.

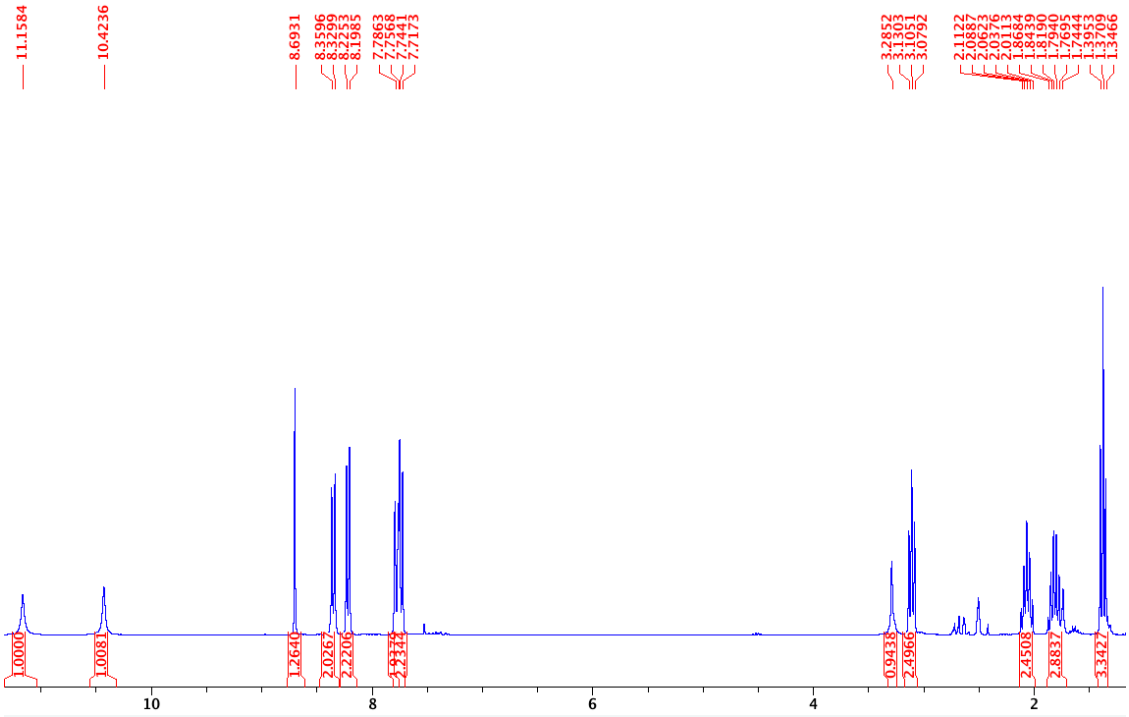

Fig. S9 ^{1}H NMR (400 MHz) spectrum of compound **5** in DMSO-d_6.

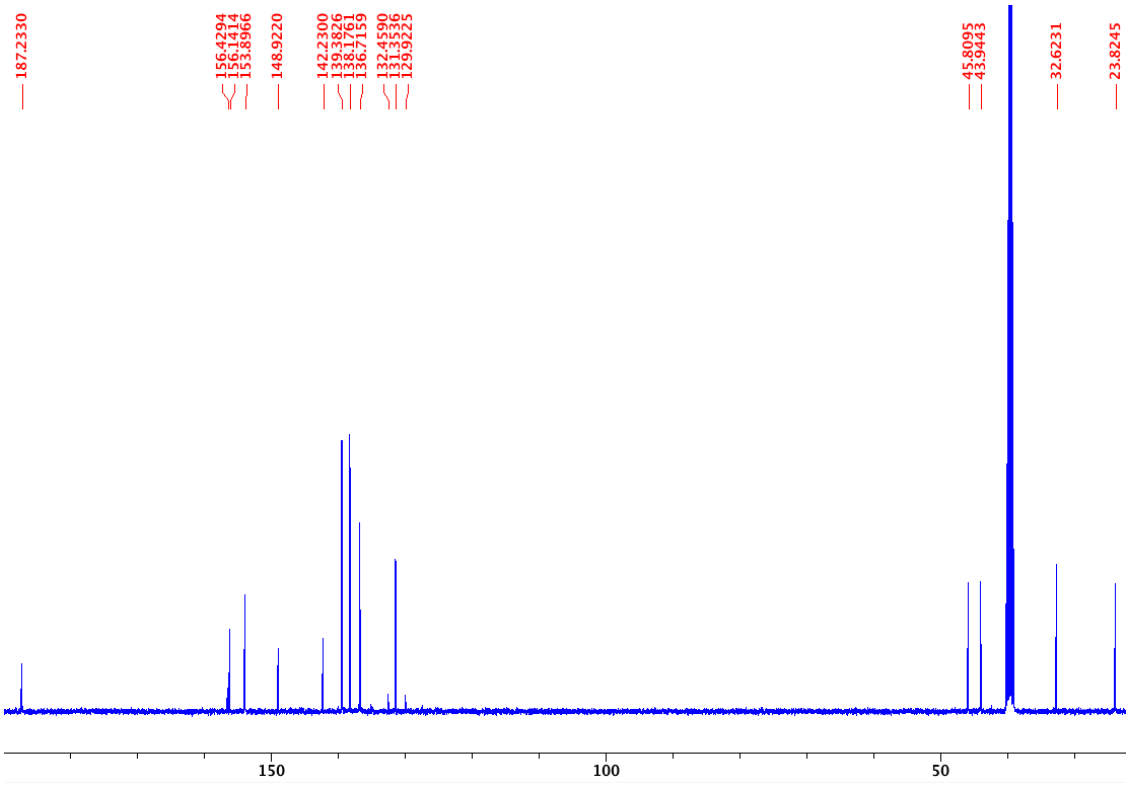

Fig. S10 ^{13}C NMR (101 MHz) spectrum of compound **5** in DMSO-d_6.

Characterisation of (*E*)-*N*-(3,5-bis(trifluoromethyl)phenyl)-2-(4-butylbenzylidene)hydrazine-1-carbothioamide 6

Afforded white solid (77% yield), mp 176-177 °C

^{1}H NMR (400 MHz, $(CD_3)_2SO$, 298 K, ppm) δ: 12.16 (s, 1H, NH^{β}), 10.46 (s, 1H, NH^{α}), 8.49 (s, 2H, Ar*H* × 2), 8.19 (s, 1H, NC*H*), 7.88 (s, 1H, Ar*H*), 7.83 (d, *J* = 8.1 Hz, 2H, Ar*H* × 2), 7.28 (d, *J* = 8.1 Hz, 2H, Ar*H* × 2), 2.62 (t, *J* = 7.6 Hz, 2H, CH_2), 1.57 (quint, *J* = 7.6 Hz, 2H, CH_2), 1.31 (sext, *J* = 7.5 Hz, 2H, CH_2), 0.90 (t, *J* = 7.5 Hz, 3H, CH_3).

^{13}C NMR (101 MHz, $(CD_3)_2SO$, 298 K, ppm) δ: 175.6, 145.2, 144.4, 141.1, 131.2, 129.7 (q, ^{2}J(C,F) = 33 Hz), 128.6, 127.8, 125.3 (q, ^{3}J(C,F) = 4 Hz), 123.3 (q, ^{1}J(C,F) = 272 Hz), 117.8 (q, ^{3}J(C,F) = 4 Hz), 34.8, 32.9, 21.7, 13.7.

^{19}F NMR (376 MHz, DMSO-d6, dppm) δ: -61.39 (s, 6F)

MS (APCI^{+}) m/z: calcd for $C_{20}H_{20}F_6N_3S$: 448.13, found: 448.10.

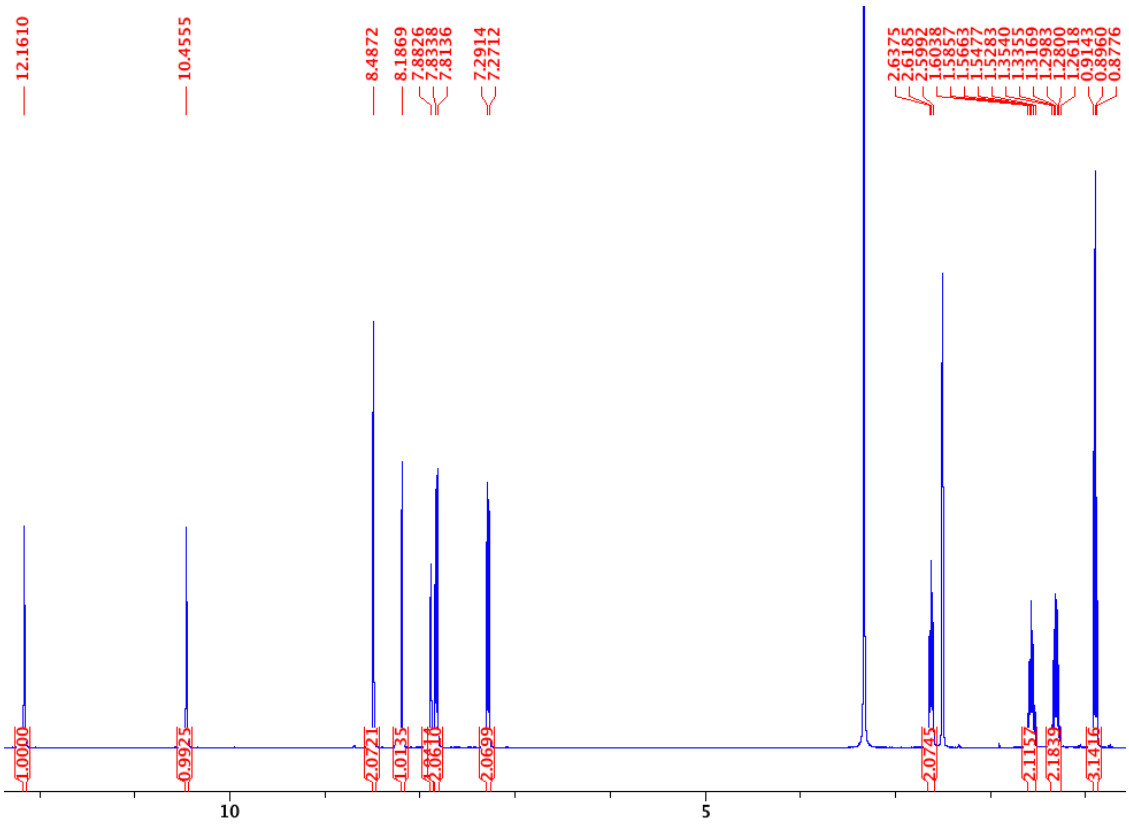

Fig. S11 ^{1}H NMR (400 MHz) spectrum of compound **6** in DMSO-d_6.

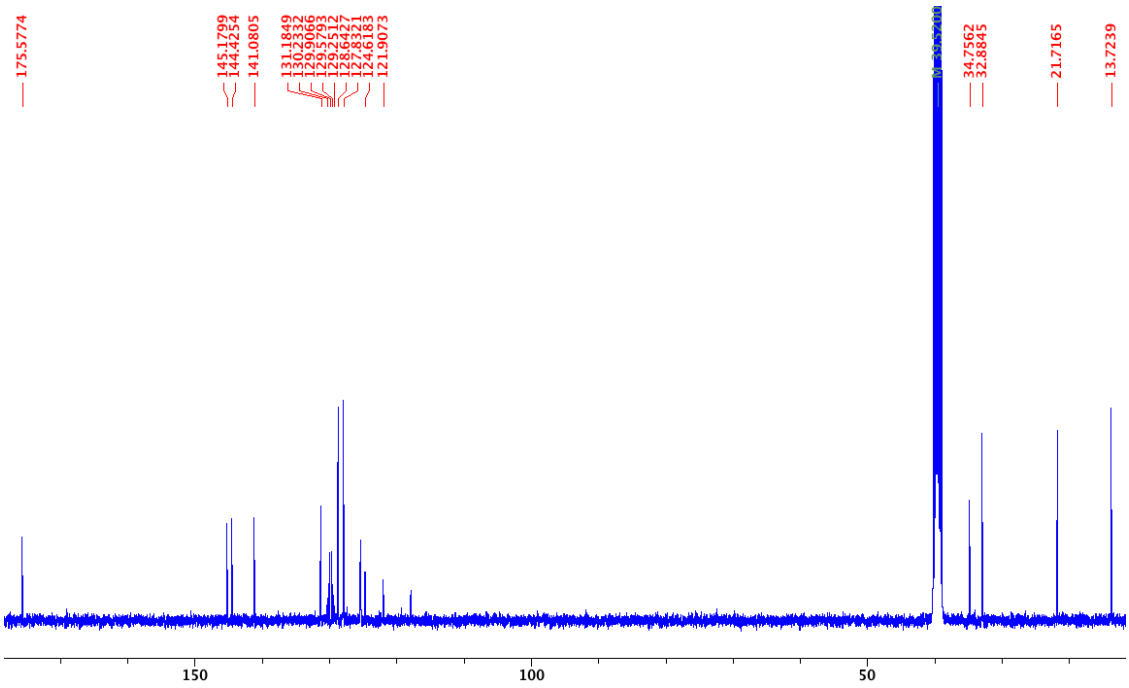

Fig. S12 ^{13}C NMR (101 MHz) spectrum of compound **6** in DMSO-d_6.

Characterisation of (*E*)-2-(4-butylbenzylidene)-*N*-(4-fluorophenyl)hydrazine-1-carbothioamide 7

Afforded white crystalline solid (88% yield), mp 137-139 °C

^{1}H NMR (400 MHz, $(CD_3)_2SO$, 298 K, ppm) δ: 11.79 (s, 1H, N*H*$^{\beta}$), 10.07 (s, 1H, N*H*$^{\alpha}$), 8.13 (s, 1H, NC*H*), 7.80 (d, *J* = 8.3 Hz, 2H, Ar*H* × 2), 7.55 (dd, *J* = 8.8, 5.1 Hz, 2H, Ar*H* × 2), 7.25 (d, *J* = 8.3 Hz, 2H, Ar*H* × 2), 7.20 (dd *J* = 9.1, 8.8 Hz, 2H, Ar*H* × 2), 2.61 (t, *J* = 7.2 Hz, 2H, C*H*$_2$), 1.56 (quint, *J* = 7.2 Hz, 2H, C*H*$_2$), 1.31 (sext, *J* = 7.2 Hz, 2H, C*H*$_2$), 0.89 (t, *J* = 7.2 Hz, 3H, C*H*$_3$).

^{13}C NMR (101 MHz, $(CD_3)_2SO$, 298 K, ppm) δ: 176.2, 159.6 (d, ^{1}J(C,F) = 242 Hz), 144.8, 143.1, 135.4 (d, ^{4}J(C,F) = 3 Hz), 131.5, 128.6, 128.1 (d, ^{3}J(C,F) = 8 Hz), 127.6, 114.6 (d, ^{2}J(C,F) = 23 Hz), 34.76, 32.93, 21.75, 13.76.

^{19}F NMR (376 MHz, DMSO-d6, dppm) δ: -117.22 (s, 1F)

MS (ESI^{+}) m/z: calcd for $C_{18}H_{21}FN_3S$: 330.14, found: 330.15; calcd for $C_{18}H_{20}FN_3SNa$: 352.13, found: 352.14.

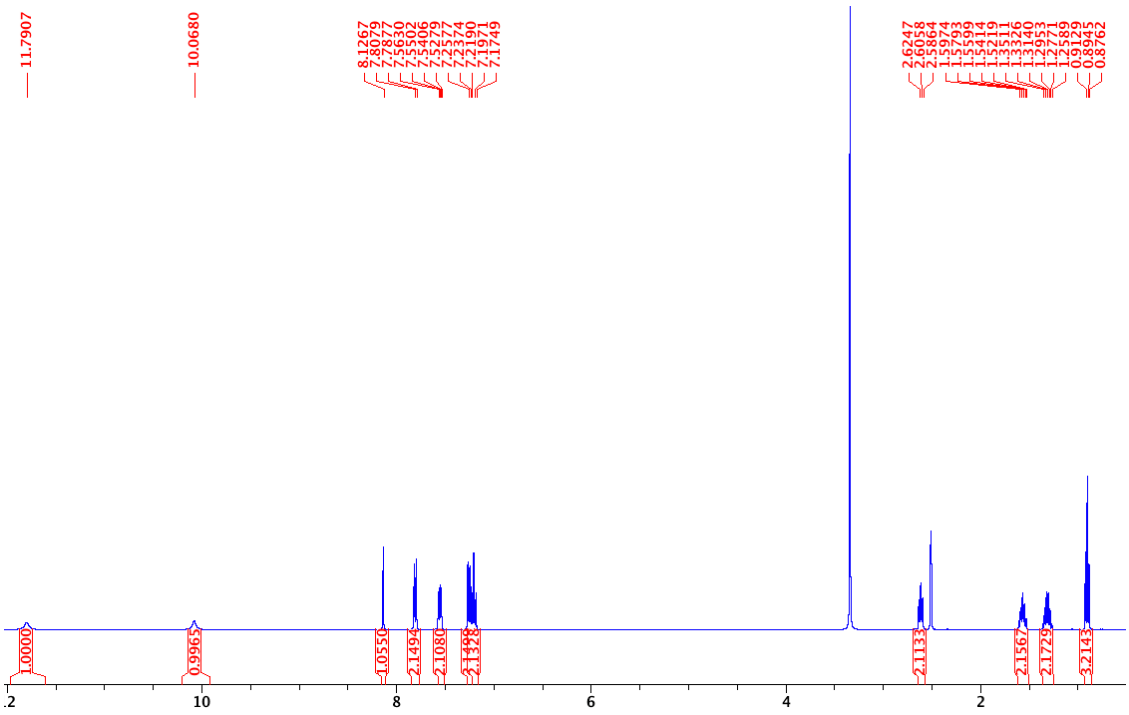

Fig. S13 ^{1}H NMR (400 MHz) spectrum of compound **7** in DMSO-d_6.

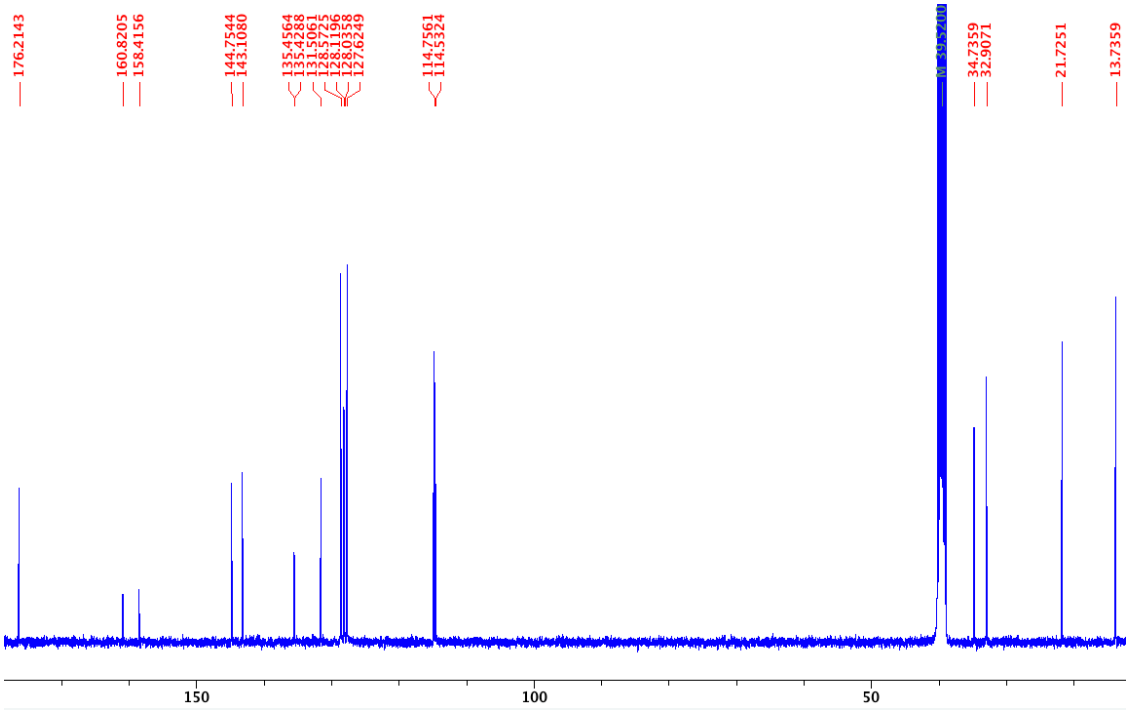

Fig. S14 ^{13}C NMR (101 MHz) spectrum of compound **7** in DMSO-d_6.

Characterisation of (E)-2-(4-butylbenzylidene)-N-(3,4,5-trifluorophenyl)hydrazine-1-carbothioamide 8

Afforded white crystalline solid (92% yield), mp 153-154 °C

^{1}H NMR (400 MHz, $(CD_3)_2SO$, 298 K, ppm) δ: 12.02 (s, 1H, N*H*$^{\beta}$), 10.16 (s, 1H, N*H*$^{\alpha}$), 8.15 (s, 1H, NC*H*), 7.80 (d, *J* = 8.0 Hz, 2H, Ar*H* × 2), 7.74 (dd, *J* = 10.0, 6.0 Hz, 2H, Ar*H* × 2), 7.27 (d, *J* = 8.0 Hz, 2H, Ar*H* × 2), 2.61 (t, *J* = 7.6 Hz, 2H, C*H*$_2$), 1.56 (quint, *J* = 7.5 Hz, 2H, C*H*$_2$), 1.31 (sext, *J* = 7.5 Hz, 2H, C*H*$_2$), 0.90 (t, *J* = 7.4 Hz, 3H, C*H*$_3$).

^{13}C NMR (101 MHz, $(CD_3)_2SO$, 298 K, ppm) δ: 175.5, 149.3 (dm, ^{1}J(C,F) = 244 Hz), 145.1, 144.0, 136.0 (d, ^{1}J(C,F) = 247 Hz), 135.4 (d, ^{3}J(C,F) = 4 Hz), 131.2, 128.6, 127.8, 109.8 (d, ^{2}J(C,F) = 23 Hz), 34.7, 32.9, 21.7, 13.7.

^{19}F NMR (376 MHz, DMSO-d6, dppm) δ: -136.18 (d, *J* = 23 Hz, 2F), -165.98 (t, *J* = 23 Hz, 1F)

MS (ESI^{+}) m/z: calcd for $C_{18}H_{19}F_3N_3S$: 366.12, found: 366.15; calcd for $C_{18}H_{18}F_3N_3SNa$: 388.11, found: 388.10.

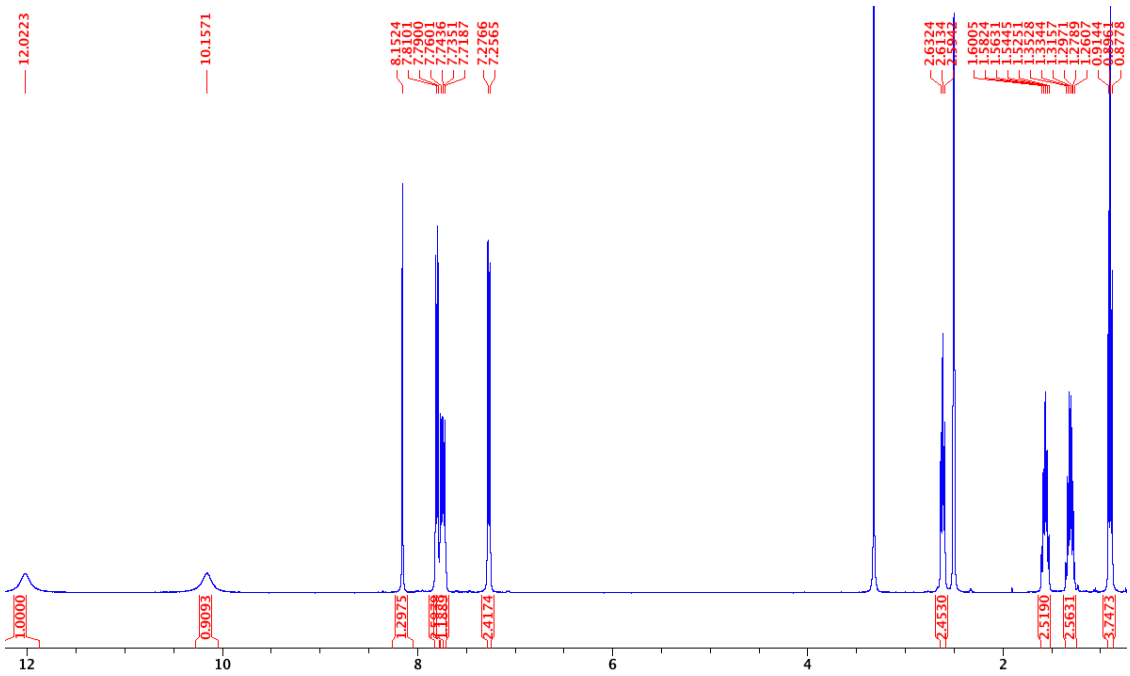

Fig. S15 ^{1}H NMR (400 MHz) spectrum of compound **8** in DMSO-*d*$_6$.

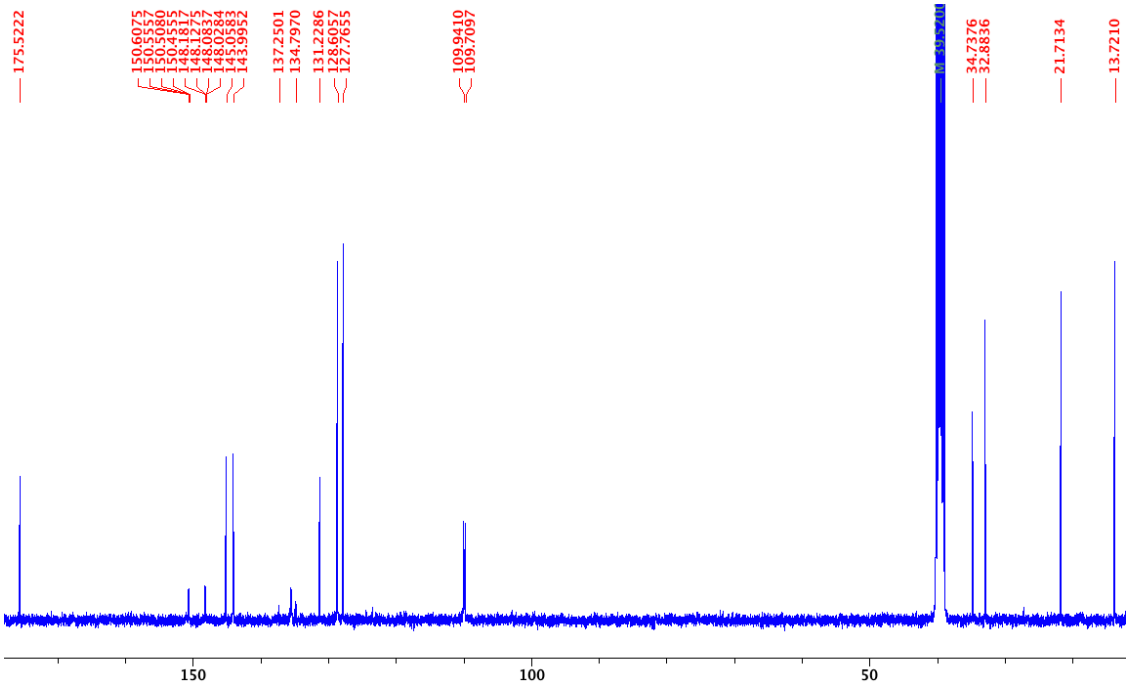

Fig. S16 ^{13}C NMR (101 MHz) spectrum of compound **8** in DMSO-d_6.

Characterisation of (*E*)-2-(4-butylbenzylidene)-*N*-(perfluorophenyl)hydrazine-1-carbothioamide 9

Afforded white solid (85% yield), mp 187-189 °C

^{1}H NMR (400 MHz, $(CD_3)_2SO$, 298 K, ppm) δ: 12.31 (s, 1H, NH^{β}), 9.93 (s, 1H, NH^{α}), 8.16 (s, 1H, NC*H*), 7.79 (d, *J* = 8.2 Hz, 2H, Ar*H* × 2), 7.27 (d, *J* = 8.2 Hz, 2H, Ar*H* × 2), 2.61 (t, *J* = 7.6 Hz, 2H, CH_2), 1.56 (quint, *J* = 7.6 Hz, 2H, CH_2), 1.31 (sext, *J* = 7.4 Hz, 2H, CH_2), 0.89 (t, *J* = 7.4 Hz, 3H, CH_3).

^{13}C NMR (101 MHz, $(CD_3)_2SO$, 298 K, ppm) δ: 177.7, 145.2, 144.6, 144.1 (d, ^{1}J(C,F) = 245 Hz), 137.2 (d, ^{1}J(C,F) = 254 Hz), 131.2, 128.7, 127.7, 115.6 (d, ^{2}J(C,F) = 15 Hz), 115.5 (d, ^{2}J(C,F) = 16 Hz), 34.8, 32.9, 21.7, 13.7.

^{19}F NMR (376 MHz, DMSO-d6, dppm) δ: -144.77 (d, *J* = 19 Hz, 2F), -155.89 (t, *J* = 22 Hz, 1F), -144.77 (t, *J* = 21 Hz, 2F).

MS (ESI^{+}) m/z: calcd for $C_{18}H_{17}F_5N_3S$: 402.11, found: 402.14; calcd for $C_{18}H_{16}F_5N_3SNa$: 424.09, found: 424.10.

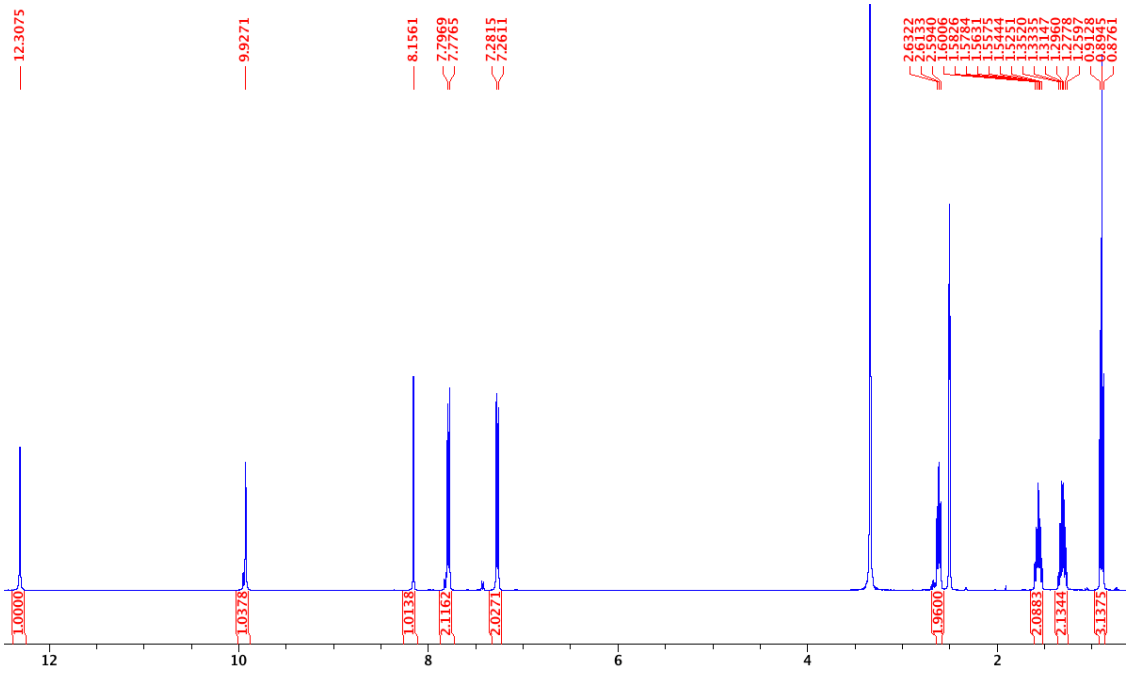

Fig. S17 ^{1}H NMR (400 MHz) spectrum of compound **9** in DMSO-d_6.

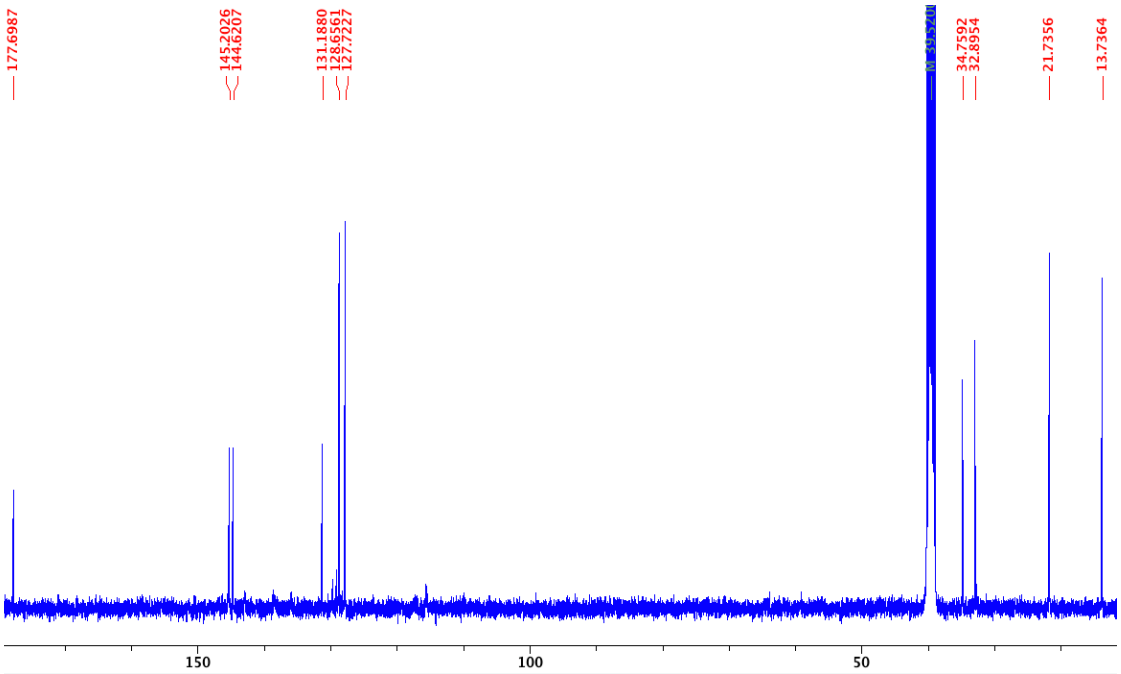

Fig. S18 ^{13}C NMR (101 MHz) spectrum of compound **9** in DMSO-d_6.

S2 ISE assay

S2.1 General Procedure for Cl^-/NO_3^- Exchange

External chloride concentrations during transport experiments were determined using a chloride-selective electrode. The electrode was calibrated against sodium chloride solutions of known concentrations prior to each experiment and the calibration was fitted against a logarithmic function: $y=A\cdot log(x)+B$, where y is the electrode read-out in mV and x is the chloride concentration in M.

A lipid film of POPC was formed from a chloroform solution under reduced pressure and dried under vacuum for at least 8 hours. The lipid film was hydrated by vortexing with a metal chloride (MCl) buffered solution (intravesicular/internal solution). The lipid suspension was then subjected to 9 freeze-thaw cycles, where the suspension was alternatingly allowed to freeze in a liquid nitrogen bath, followed by thawing in a water bath. The lipid suspension was allowed to age for 30 minutes at room temperature and was extruded 25 times through a 200 nm polycarbonate membrane using a extruder set. The unilamellar vesicles (LUVs) were dialyzed against the extravesicular/external buffered solution for a minimum of 2 hours to remove unencapsulated MCl salts. The lipid solution obtained after dialysis was diluted to a standard volume of 10 mL with the external buffered solution to obtain the lipid stock solution with a known lipid concentration.

The internal and external solutions vary from experiment to experiment. The buffers for various pHs were prepared with a constant buffer concentration (5.0 mM, citrate buffer for pH 4.5 and phosphate buffer for pH 7.2) and total ionic strength (500 mM) for both intra- and extravesicular solutions. Typically, for each measurement, the lipid stock solution was diluted with the external buffered solution to a standard volume (5.0 mL) with a lipid concentration of 1.0 mM. A DMSO solution (10 μL) of the test compound (carrier) was added to the liposome solution to start the experiment and the chloride efflux was monitored using a chloride-selective electrode. At 5 minutes, the detergent solution (50 μL) was added to lyse the vesicles, and the total chloride reading was taken at 7 min. The initial value was set as 0% chloride efflux and the final chloride reading (at 7 minutes) was set as 100% chloride efflux, to normalize the collected data from each measurement.

S2.2 General Procedure for cationophore-coupled assay

Chloride concentrations during transport experiments were monitored using a chloride-selective electrode. POPC LUVs (mean diameter 200 nm) with internal KCl and external K_2SO_4 were prepared as follows. A lipid film of POPC was formed from a chloroform solution under reduced pressure and dried under vacuum for at least 8 hours. The lipid film was hydrated by vortexing with the intravesicular KCl (300 mM) solution. The lipid suspension was then subjected to 9 freezethaw cycles, where the suspension was alternatingly allowed to freeze in a liquid nitrogen bath, followed by thawing in a water bath. The lipid suspension was allowed to age for 30 minutes at room temperature and was extruded 25 times through a 200 nm polycarbonate membrane using an extruder set. The resulting large unilamellar vesicles (LUVs) with a mean diameter of 200 nm were dialyzed against the extravesicular K_2SO_4 (100 mM) for a minimum of 2 hours to remove unencapsulated KCl salts. The lipid solution obtained after dialysis was diluted to a standard volume (10 mL) with the extravesicular buffered solution to obtain the lipid stock solution with a known lipid concentration.

A DMSO solution (10 μL) of the anionophore was added to the liposome solution to start the experiment and the chloride efflux was monitored using a chloride-sensitive electrode. When a cationophore (valinomycin or monensin) was used, a DMSO solution of the cationophore (0.5 mM, 10 μL) was added to the liposome solution prior to the addition of the test anionophore. At 5 min, the detergent solution (50 μL) was added to lyse the vesicles, and the total chloride reading was taken at 7 min. The initial value was set at 0% chloride efflux and the final chloride reading (at 7 minutes) was set as 100% chloride efflux, to normalise the collected data from each measurement. The KCl assay involves two complementary cationophores, monensin and valinomycin, which can determine whether the transport process is electrogenic chloride transport or electroneutral H^+/Cl^- cotransport. An electrogenic processes result in a net alteration of charge across the membrane due to ion transport, whereas electroneutral process has a charge balance that can be achieved with transport of a species with the same charge or cotransport of a species with opposite charge. Monensin functions as a M^+/H^+ antiporter in the lipid bilayer as the deprotonated monensin is unable to diffuse through the membrane unless it is binding a cation, thus it can facilitate electroneutral transport. Valinomycin can only facilitate electrogenic transport, the anionphore transports Cl^- coupled with K^+ transport mediated by

valinomycin. Chloride efflux is measured by ISE from POPC LUVs loaded with KCl (300 mM) and suspended in K_2SO_4 (100 mM), adjusted to pH 4.5 with KOH in citrate (5.0 mM) or pH 7.2 in phosphate (5.0 mM). Either monensin (0.1 mol%) or valinomycin (0.1 mol%) are added in combination with an anionophore and chloride efflux is driven by the large chloride concentration gradient.

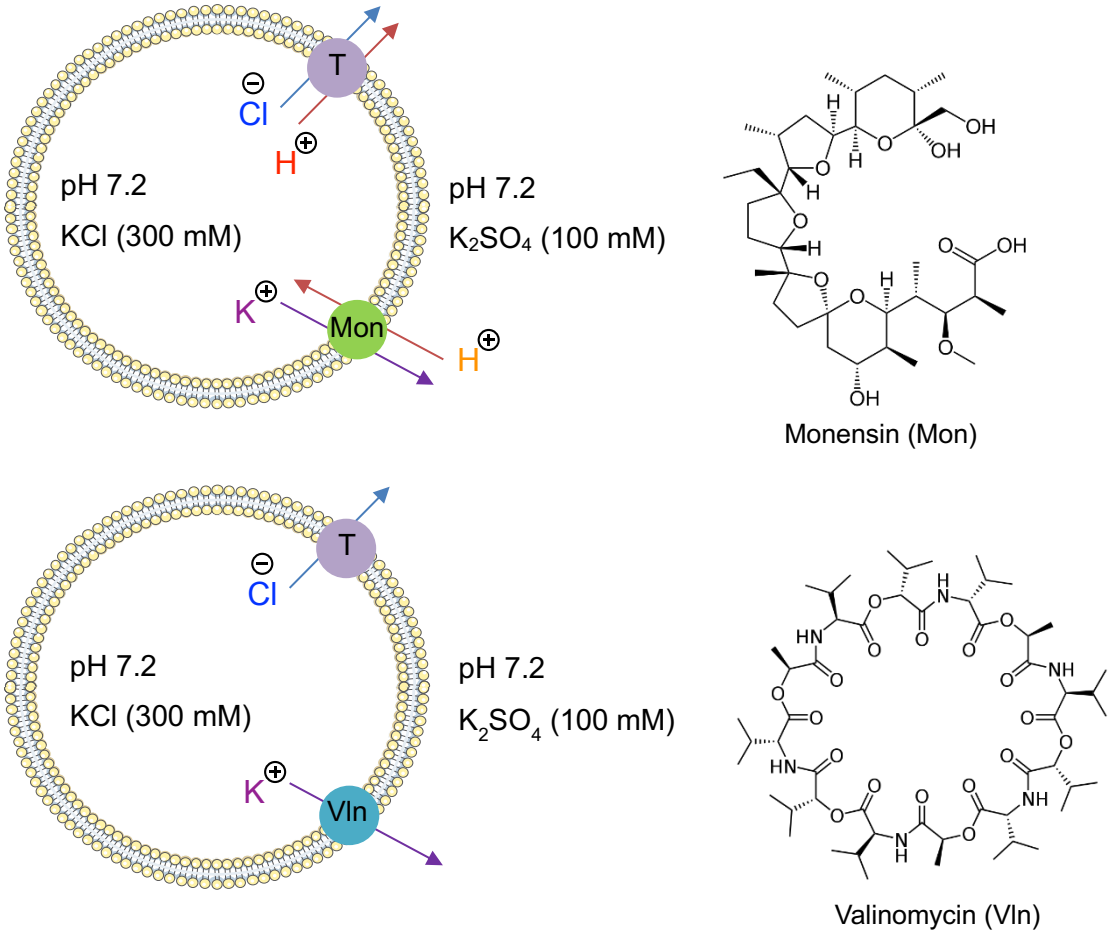

Fig. S19 Illustration of Cationophore coupled assay with monensin and valinomycin.

S2.4 Cl^-/NO_3^- exchange assay data and Hill analysis

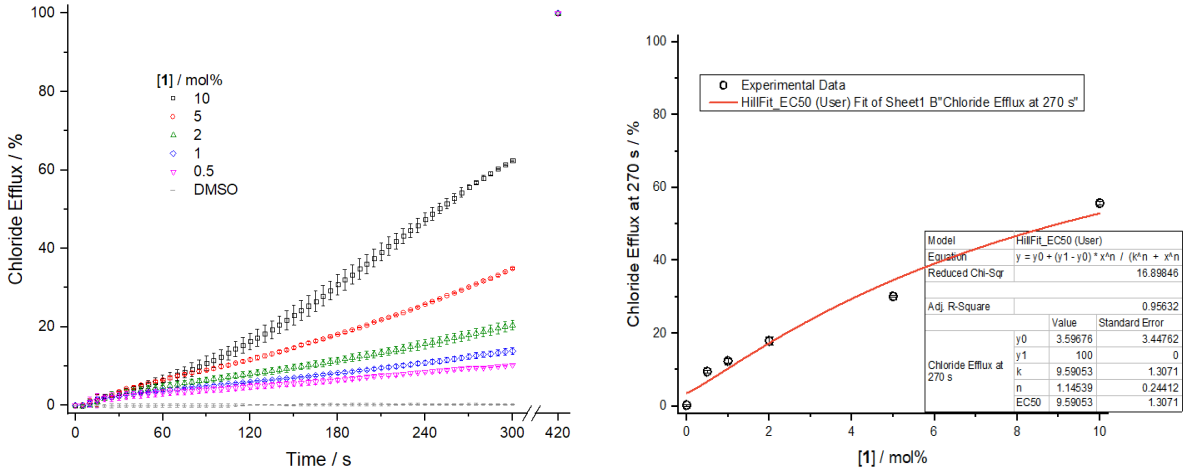

Fig. S20 Plots for Hill analysis of chloride efflux (Cl^-/NO_3^- exchange) at 270 s, mediated by compound **1** at pH 7.2. Each data point represents the average of two or three repeat measurements with error bars indicating the standard deviation.

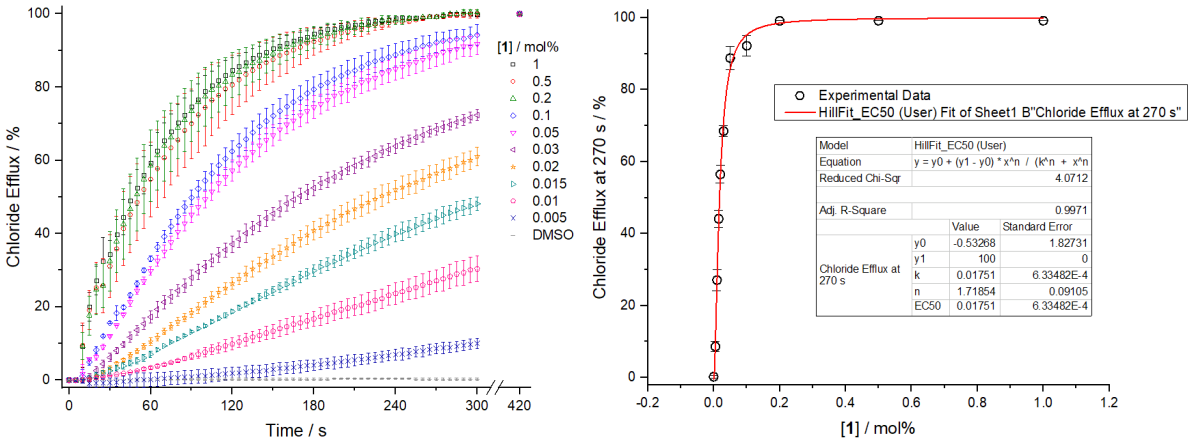

Fig. S21 Plots for Hill analysis of chloride efflux (Cl^-/NO_3^- exchange) at 270 s, mediated by compound **1** at pH 4.5. Each data point represents the average of two or three repeat measurements with error bars indicating the standard deviation.

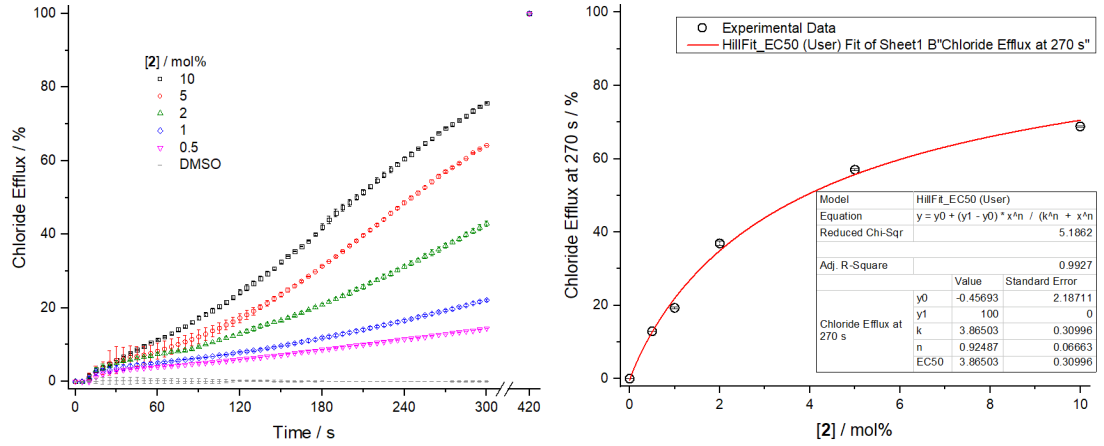

Fig. S22 Plots for Hill analysis of chloride efflux (Cl^-/NO_3^- exchange) at 270 s, mediated by compound **2** at pH 7.2. Each data point represents the average of two or three repeat measurements with error bars indicating the standard deviation.

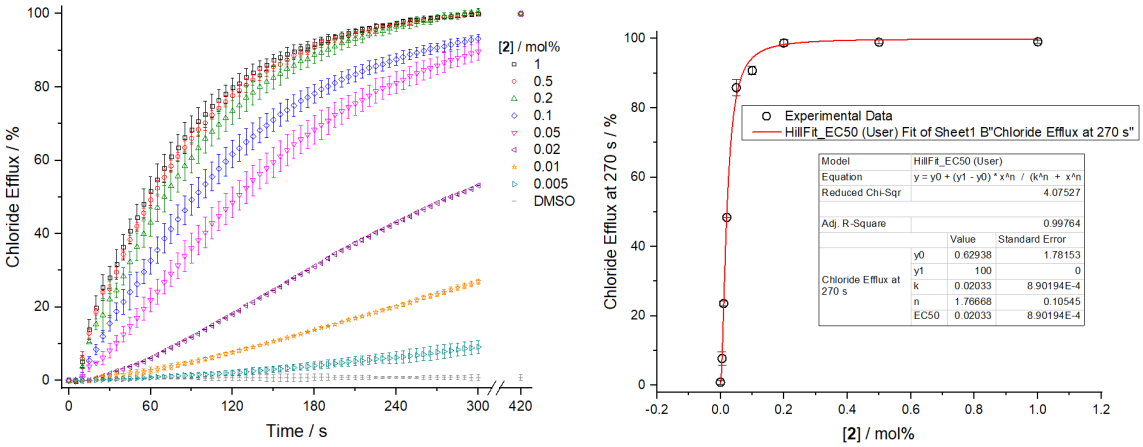

Fig. S23 Plots for Hill analysis of chloride efflux (Cl^-/NO_3^- exchange) at 270 s, mediated by compound **2** at pH 4.5. Each data point represents the average of two or three repeat measurements with error bars indicating the standard deviation.

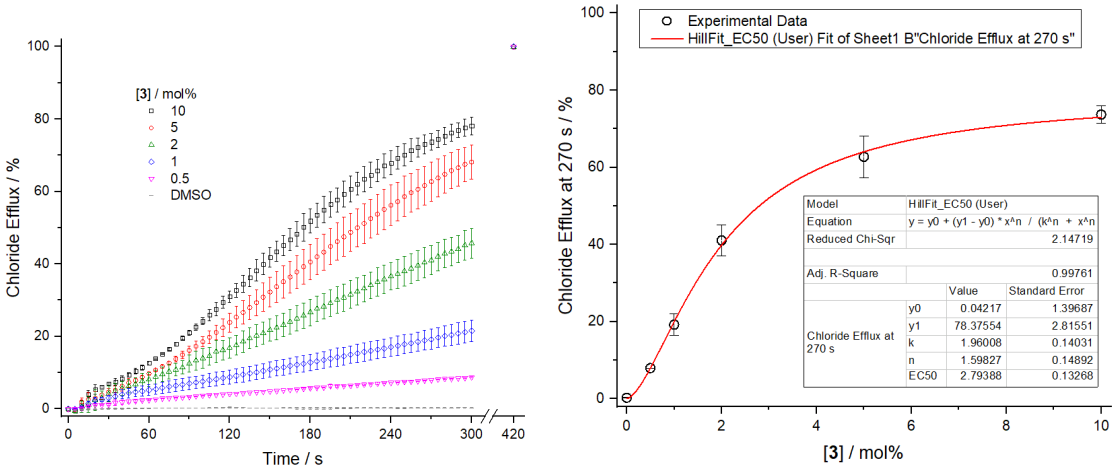

Fig. S24 Plots for Hill analysis of chloride efflux (Cl^-/NO_3^- exchange) at 270 s, mediated by compound **3** at pH 7.2. Each data point represents the average of two or three repeat measurements with error bars indicating the standard deviation.

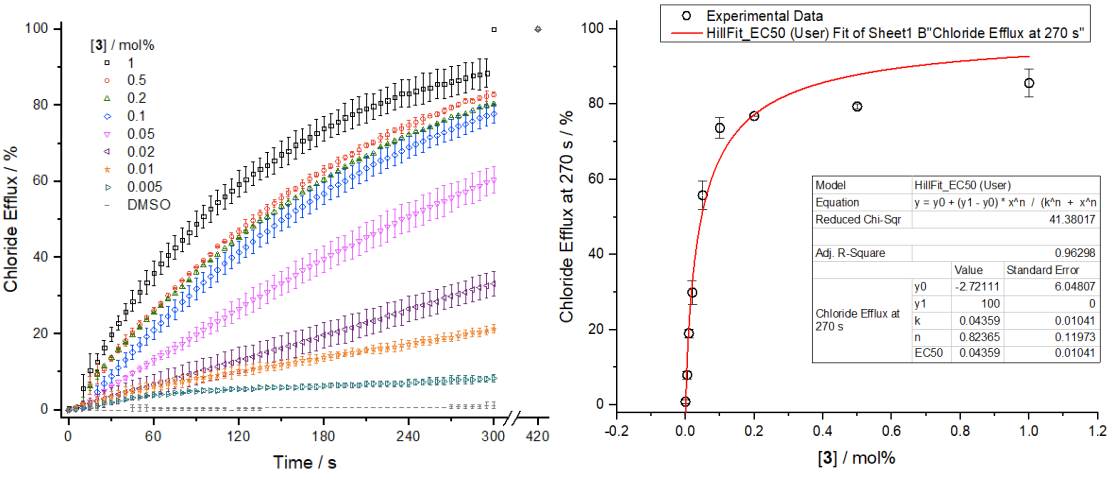

Fig. S25 Plots for Hill analysis of chloride efflux (Cl^-/NO_3^- exchange) at 270 s, mediated by compound **3** at pH 4.5. Each data point represents the average of two or three repeat measurements with error bars indicating the standard deviation.

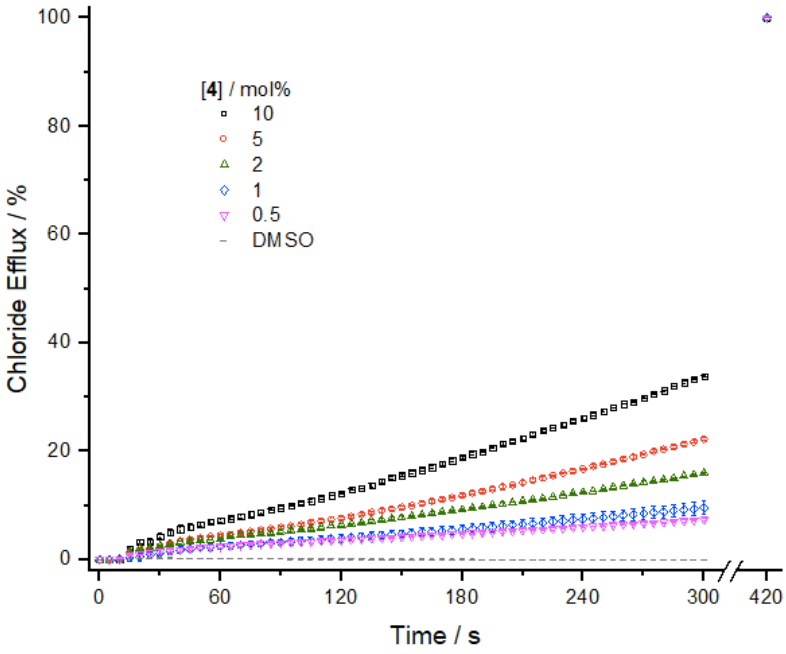

Fig. S26 Plots for Hill analysis of chloride efflux (Cl^-/NO_3^- exchange) at 270 s, mediated by compound **4** at pH 4.5. Each data point represents the average of two or three repeat measurements with error bars indicating the standard deviation.

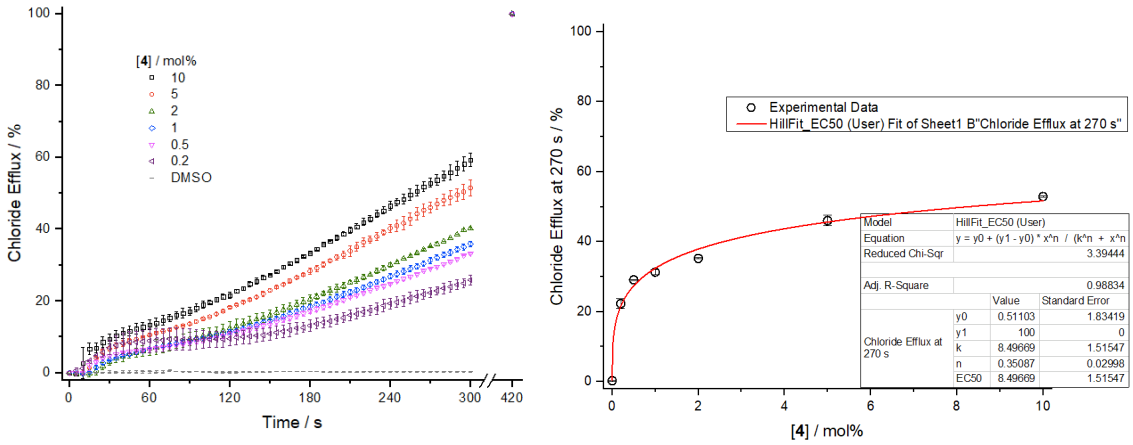

Fig. S27 Plots for attempted Hill analysis of chloride efflux (Cl^-/NO_3^- exchange) at 270 s, mediated by compound **4** at pH 7.2. Each data point represents the average of two or three repeat measurements with error bars indicating the standard deviation.

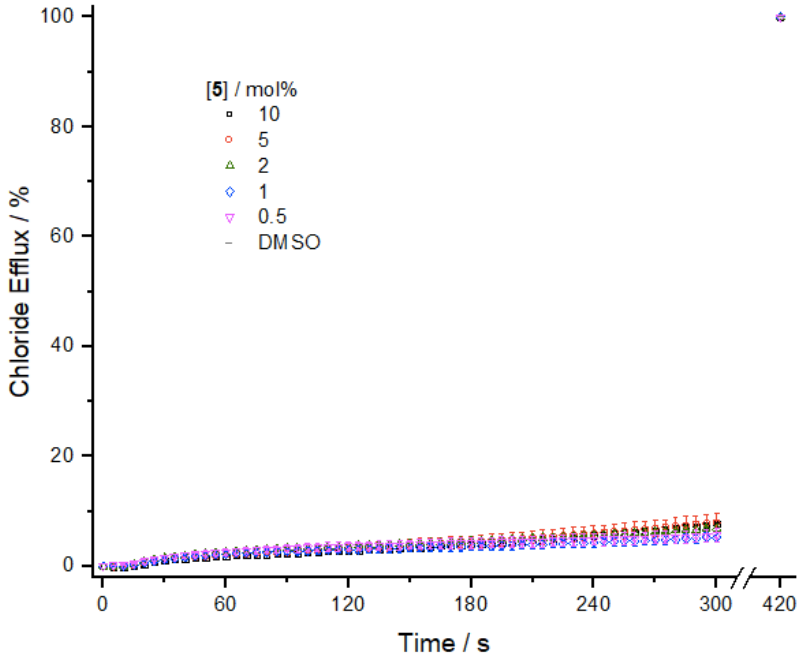

Fig. S28 Plots for attempted Hill analysis of chloride efflux (Cl^-/NO_3^- exchange) at 270 s, mediated by compound **5** at pH 7.2. Each data point represents the average of two or three repeat measurements with error bars indicating the standard deviation.

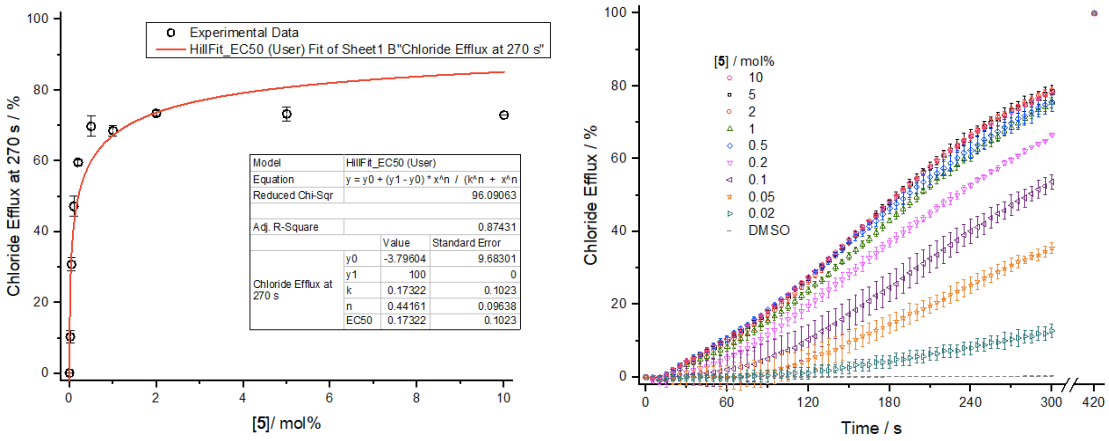

Fig. S29 Plots for Hill analysis of chloride efflux (Cl^-/NO_3^- exchange) at 270 s, mediated by compound **5** at pH 4.5. Each data point represents the average of two or three repeat measurements with error bars indicating the standard deviation.

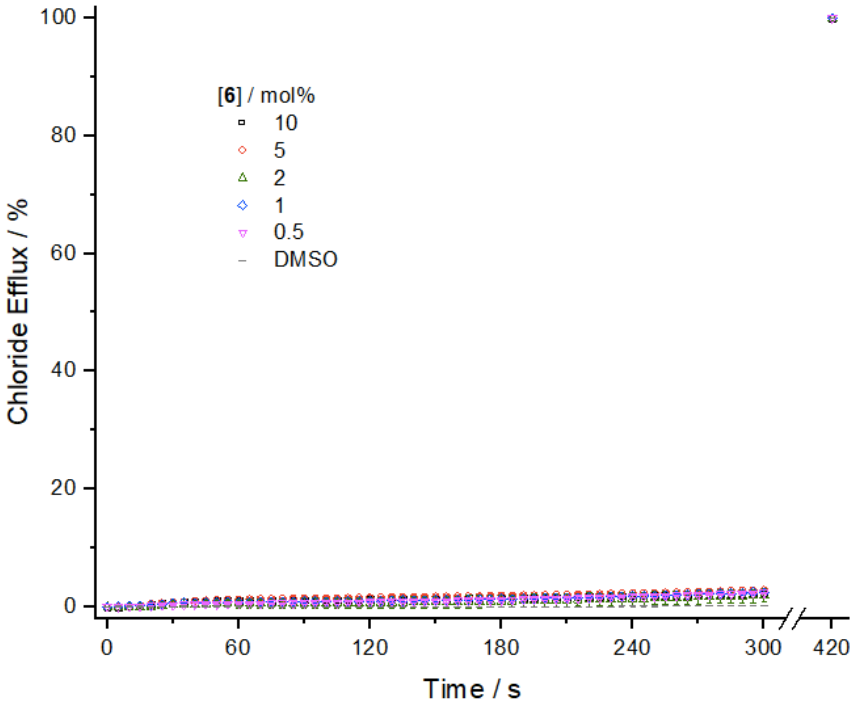

Fig. S30 Plots for attempted Hill analysis of chloride efflux (Cl^-/NO_3^- exchange) at 270 s, mediated by compound **6** at pH 7.2. Each data point represents the average of two or three repeat measurements with error bars indicating the standard deviation.

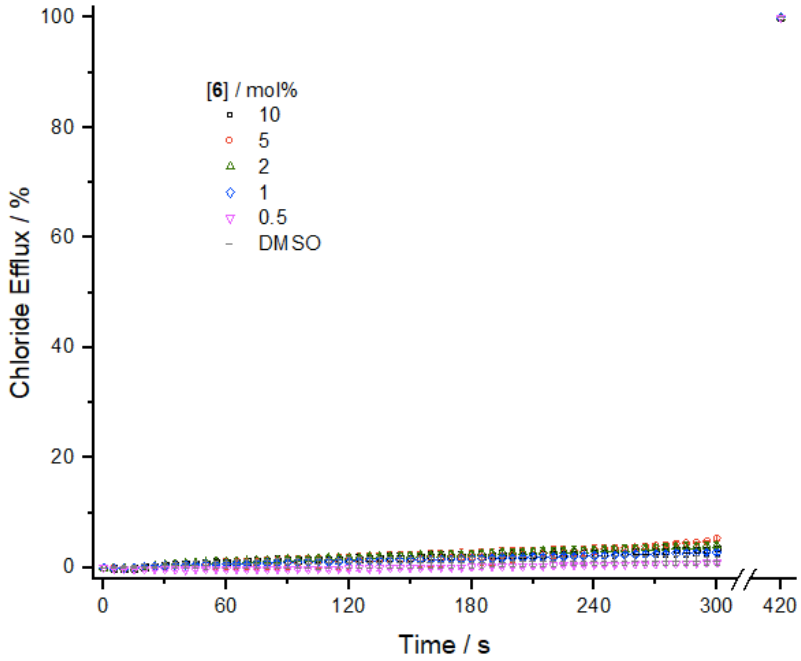

Fig. S31 Plots for attempted Hill analysis of chloride efflux (Cl^-/NO_3^- exchange) at 270 s, mediated by compound **6** at pH 4.5. Each data point represents the average of two or three repeat measurements with error bars indicating the standard deviation.

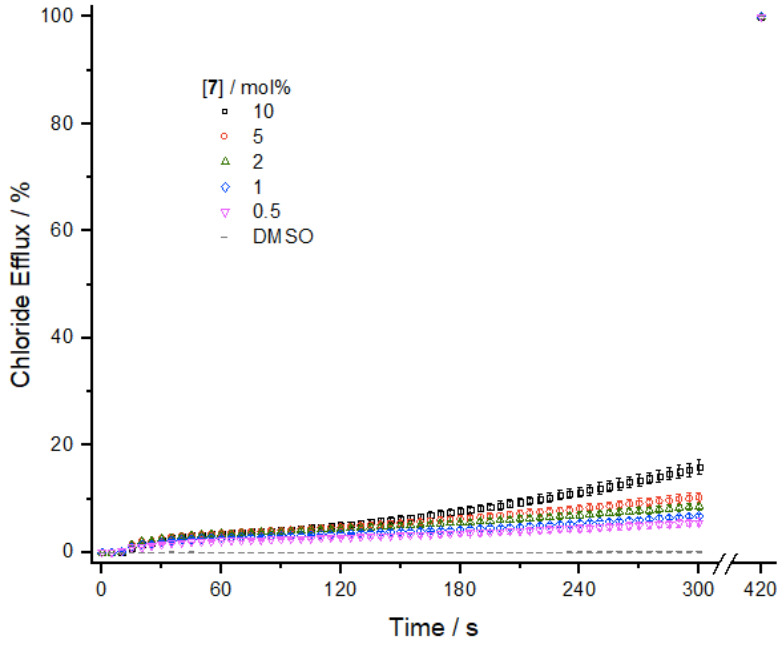

Fig. S32 Plots for attempted Hill analysis of chloride efflux (Cl^-/NO_3^- exchange) at 270 s, mediated by compound **7** at pH 7.2. Each data point represents the average of two or three repeat measurements with error bars indicating the standard deviation.

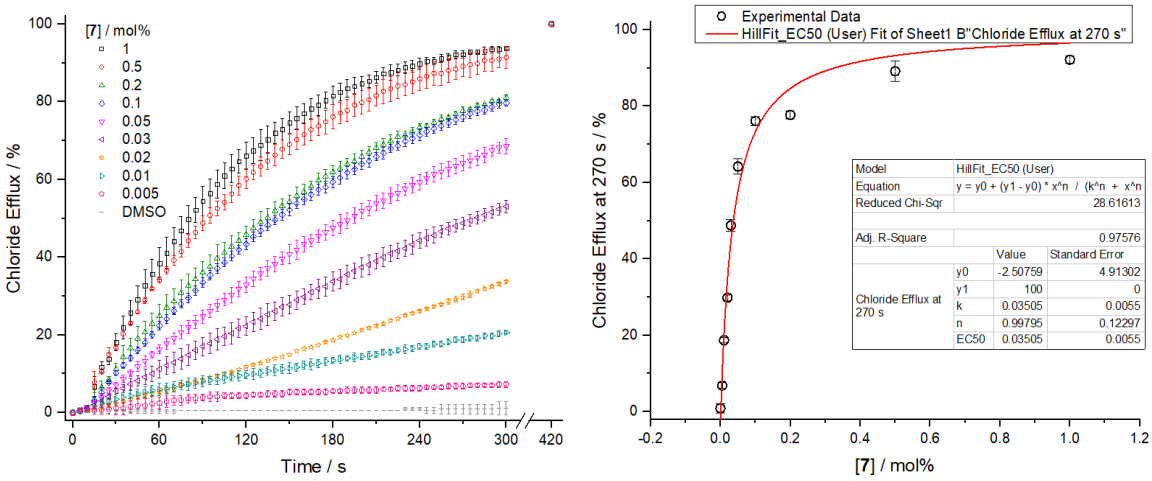

Fig. S33 Plots for Hill analysis of chloride efflux (Cl^-/NO_3^- exchange) at 270 s, mediated by compound **7** at pH 4.5. Each data point represents the average of two or three repeat measurements with error bars indicating the standard deviation.

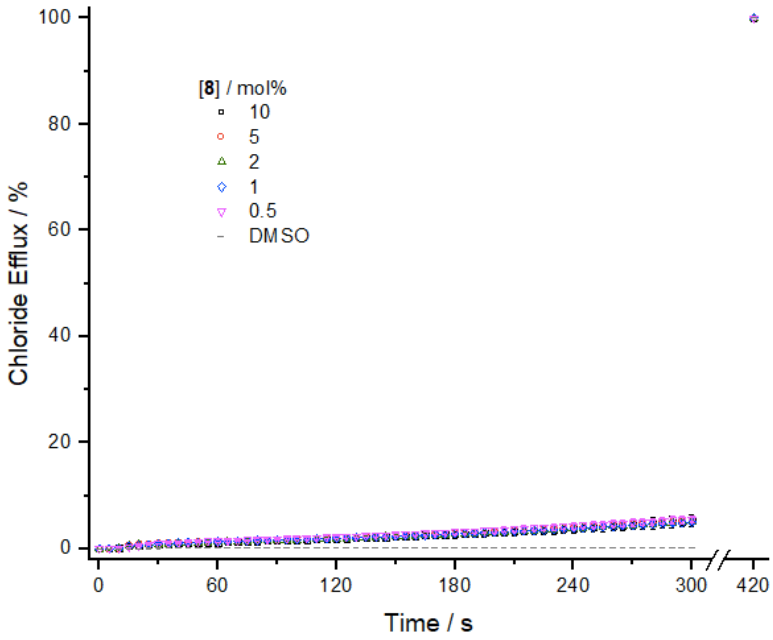

Fig. S34 Plots for attempted Hill analysis of chloride efflux (Cl^-/NO_3^- exchange) at 270 s, mediated by compound **8** at pH 7.2. Each data point represents the average of two or three repeat measurements with error bars indicating the standard deviation.

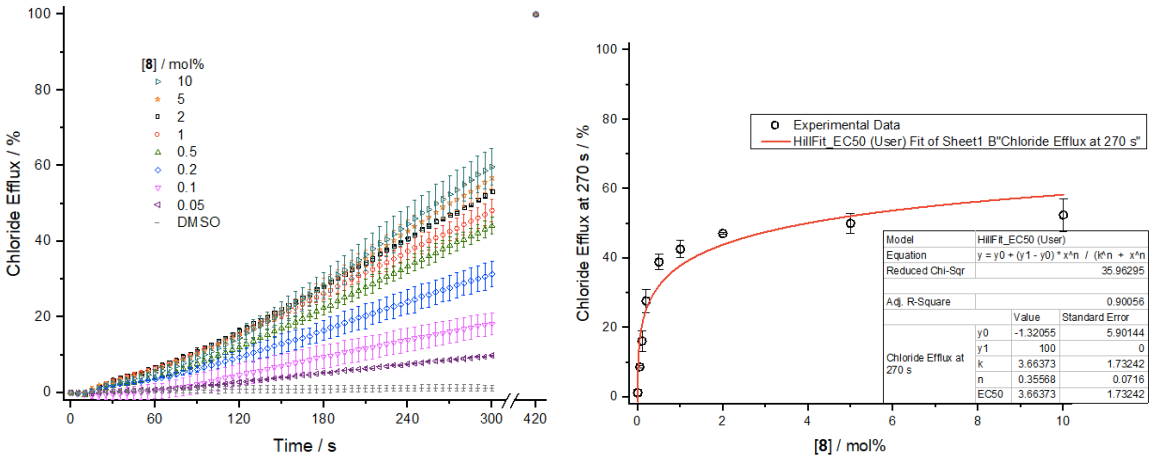

Fig. S35 Plots for Hill analysis of chloride efflux (Cl^-/NO_3^- exchange) at 270 s, mediated by compound **8** at pH 4.5. Each data point represents the average of two or three repeat measurements with error bars indicating the standard deviation.

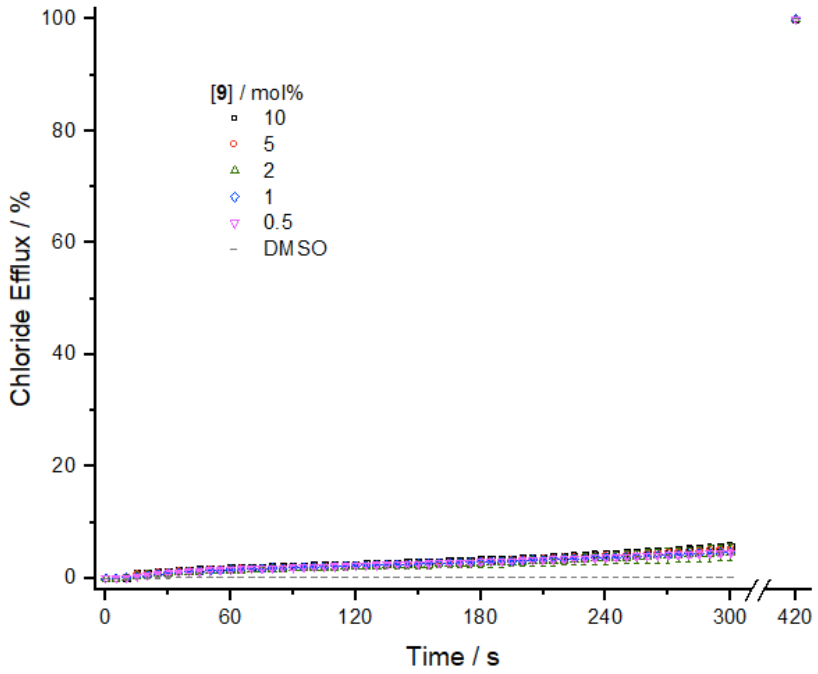

Fig. S36 Plots for attempted Hill analysis of chloride efflux (Cl^-/NO_3^- exchange) at 270 s, mediated by compound **9** at pH 7.2. Each data point represents the average of two or three repeat measurements with error bars indicating the standard deviation.

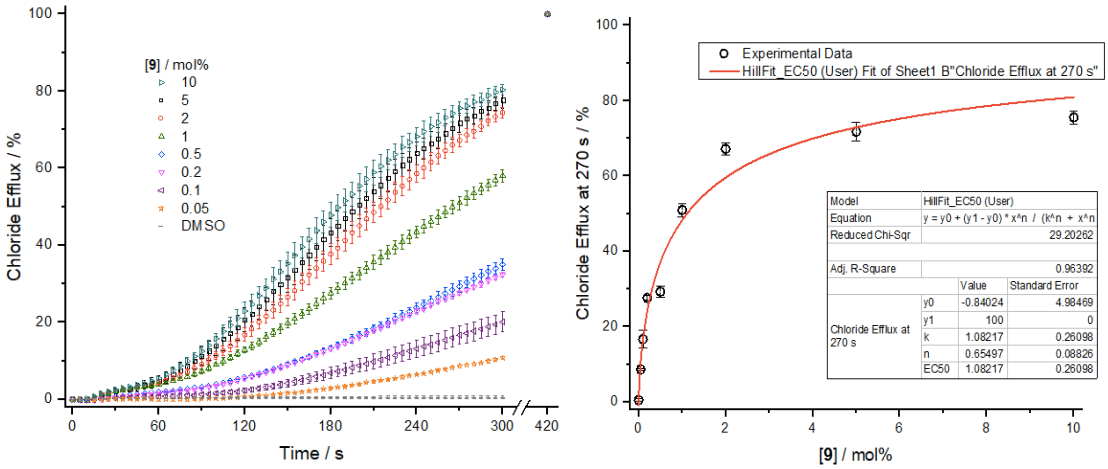

Fig. S37 Plots for Hill analysis of chloride efflux (Cl^-/NO_3^- exchange) at 270 s, mediated by compound **9** at pH 4.5. Each data point represents the average of two or three repeat measurements with error bars indicating the standard deviation.

S2.5 Cationophore-coupled assay data

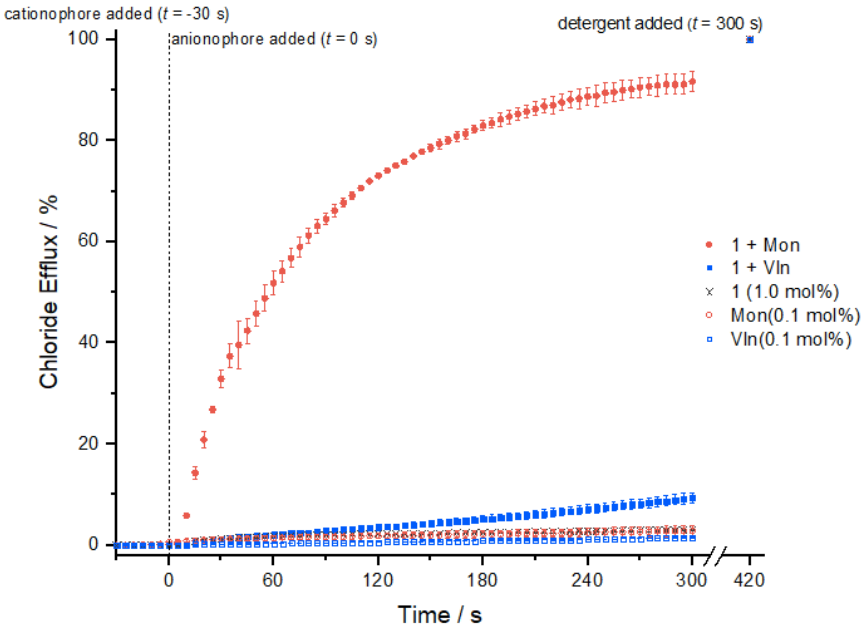

Fig. S38 Plot for chloride efflux mediated by compound **1** (1 mol%) in the presence of monensin and valinomycin at pH 7.2. Each data point represents the average of three repeat measurements with error bars indicating the standard deviation.

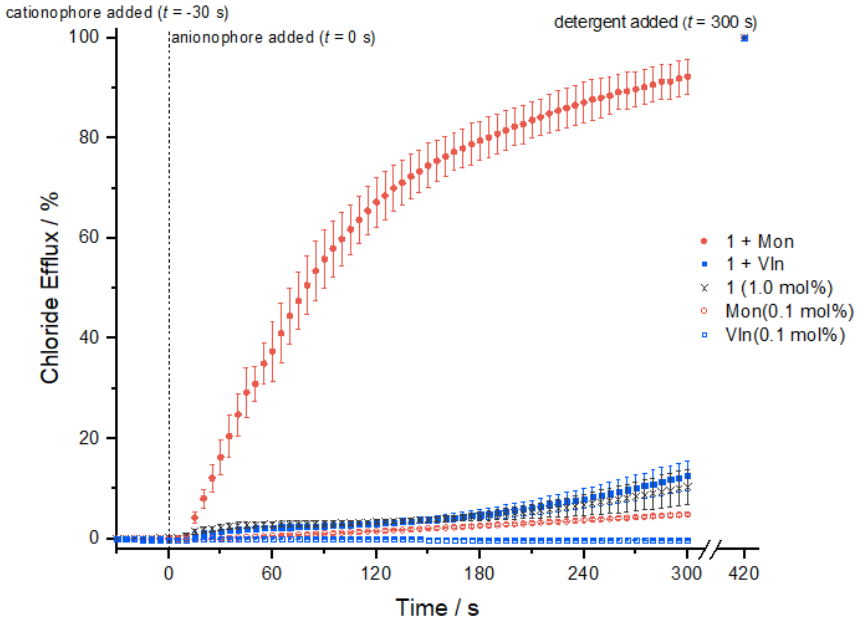

Fig. S39 Plot for chloride efflux mediated by compound **1** (1 mol%) in the presence of monensin and valinomycin at pH 4.5. Each data point represents the average of three repeat measurements with error bars indicating the standard deviation.

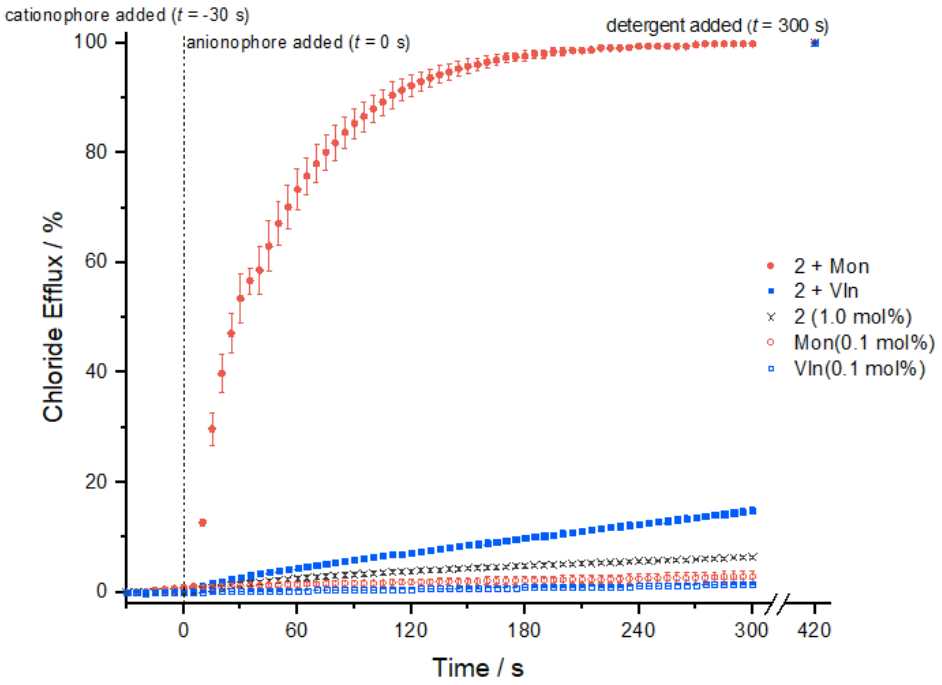

Fig. S40 Plot for chloride efflux mediated by compound **2** (1 mol%) in the presence of monensin and valinomycin at pH 7.2. Each data point represents the average of three repeat measurements with error bars indicating the standard deviation.

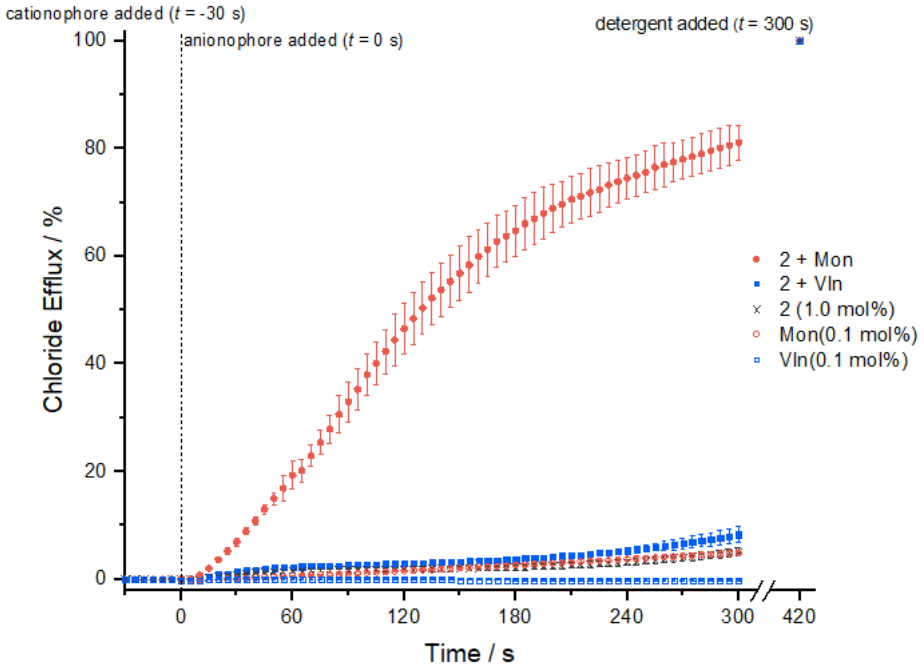

Fig. S41 Plot for chloride efflux mediated by compound **2** (1 mol%) in the presence of monensin and valinomycin at pH 4.5. Each data point represents the average of three repeat measurements with error bars indicating the standard deviation.

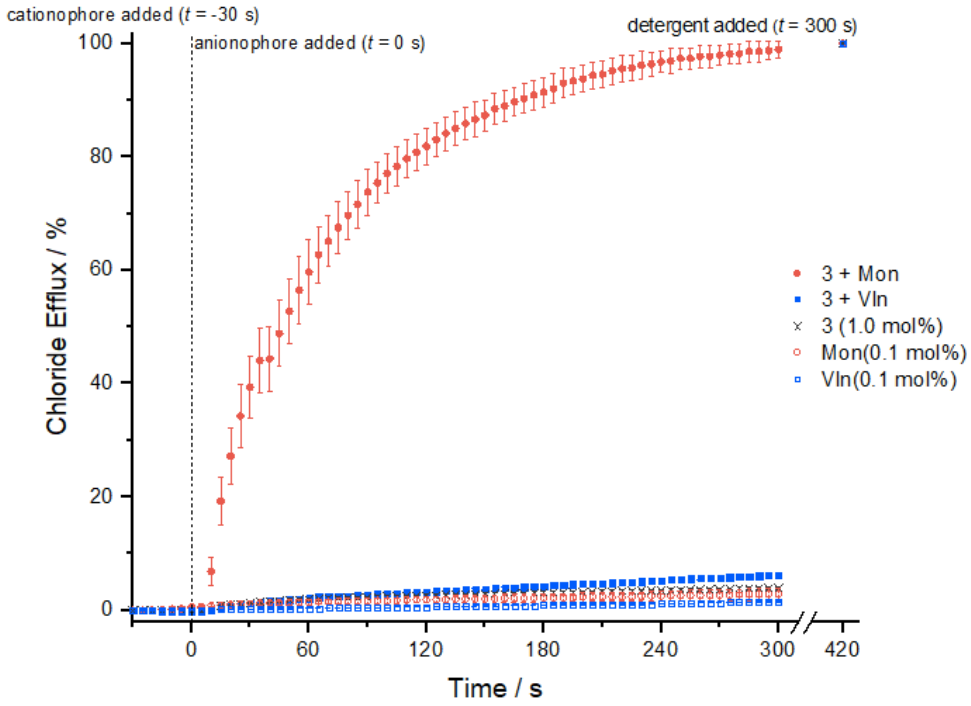

Fig. S42 Plot for chloride efflux mediated by compound **3** (1 mol%) in the presence of monensin and valinomycin at pH 7.2. Each data point represents the average of three repeat measurements with error bars indicating the standard deviation.

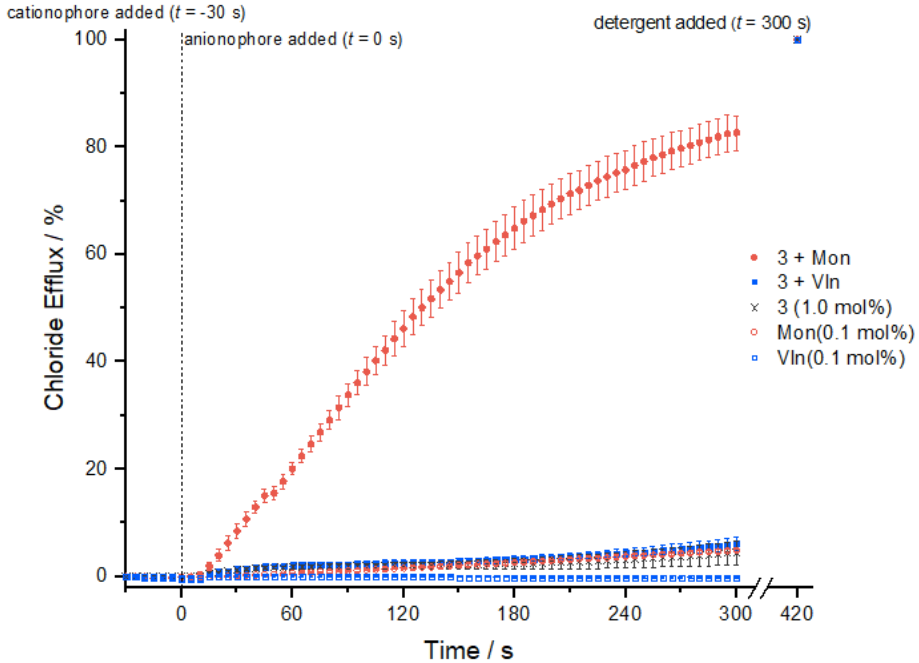

Fig. S43 Plot for chloride efflux mediated by compound **3** (1 mol%) in the presence of monensin and valinomycin at pH 4.5. Each data point represents the average of three repeat measurements with error bars indicating the standard deviation.

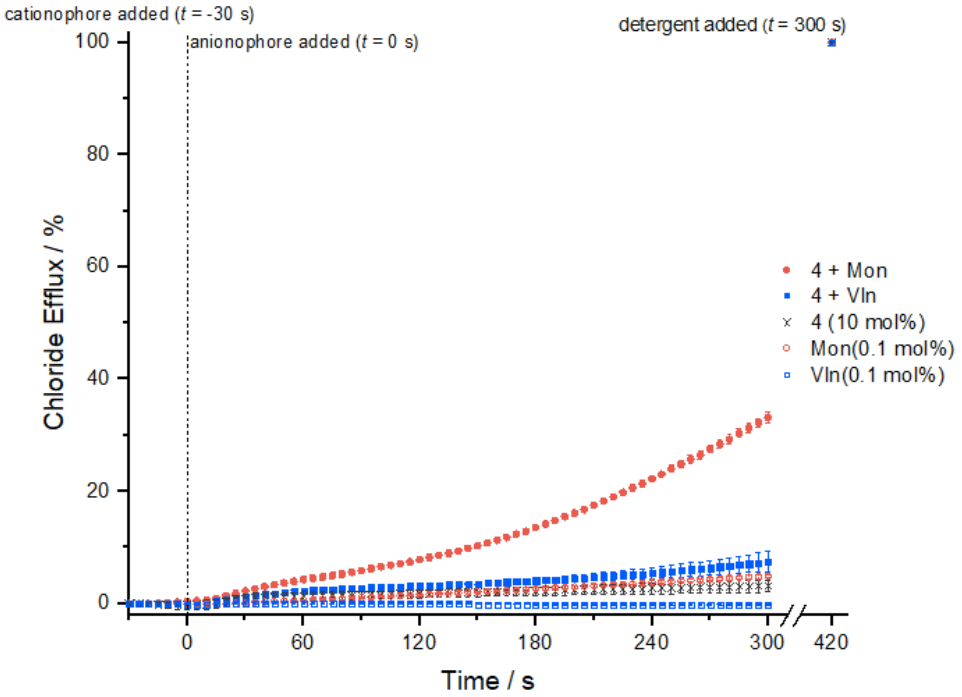

Fig. S44 Plot for chloride efflux mediated by compound **4** (10 mol%) in the presence of monensin and valinomycin at pH 7.2. Each data point represents the average of three repeat measurements with error bars indicating the standard deviation.

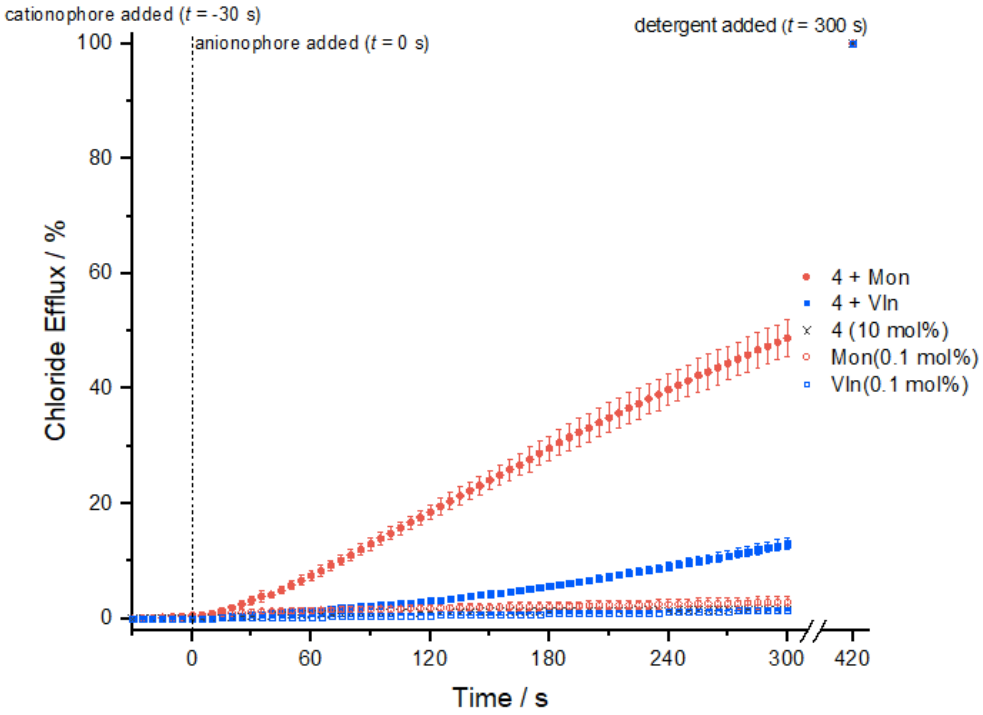

Fig. S45 Plot for chloride efflux mediated by compound **4** (10 mol%) in the presence of monensin and valinomycin at pH 4.5. Each data point represents the average of three repeat measurements with error bars indicating the standard deviation.

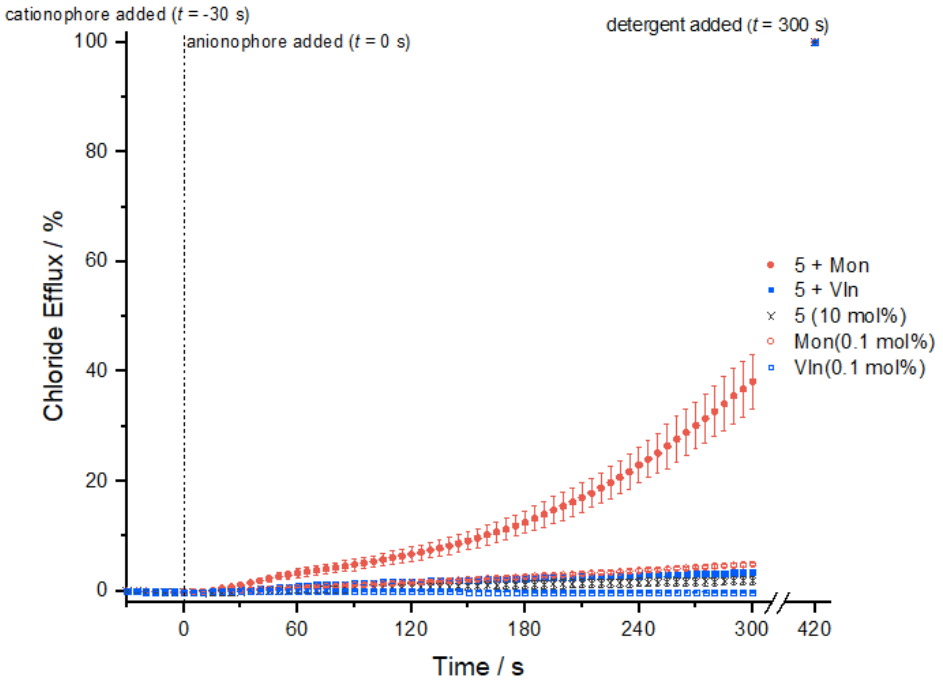

Fig. S46 Plot for chloride efflux mediated by compound **5** (10 mol%) in the presence of monensin and valinomycin at pH 7.2. Each data point represents the average of three repeat measurements with error bars indicating the standard deviation.

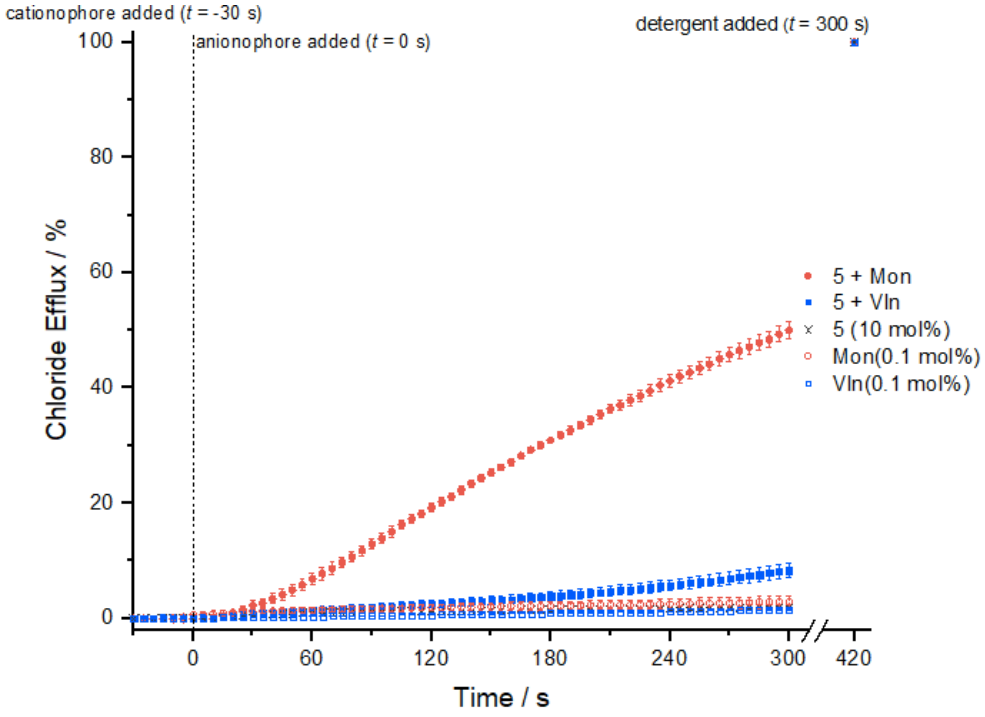

Fig. S47 Plot for chloride efflux mediated by compound **5** (10 mol%) in the presence of monensin and valinomycin at pH 4.5. Each data point represents the average of three repeat measurements with error bars indicating the standard deviation.

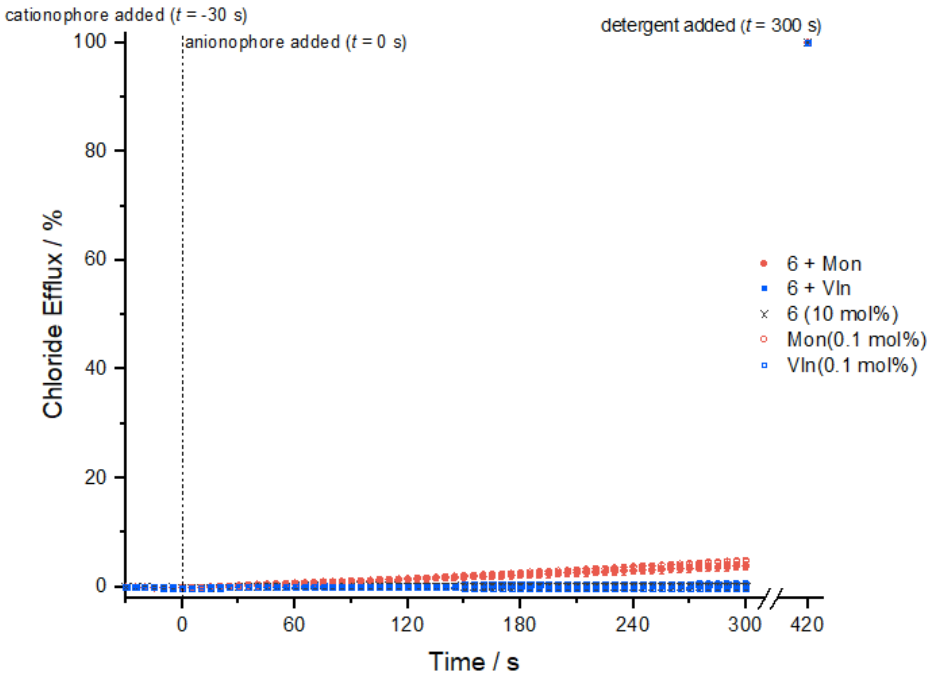

Fig. S48 Plot for chloride efflux mediated by compound **6** (10 mol%) in the presence of monensin and valinomycin at pH 7.2. Each data point represents the average of three repeat measurements with error bars indicating the standard deviation.

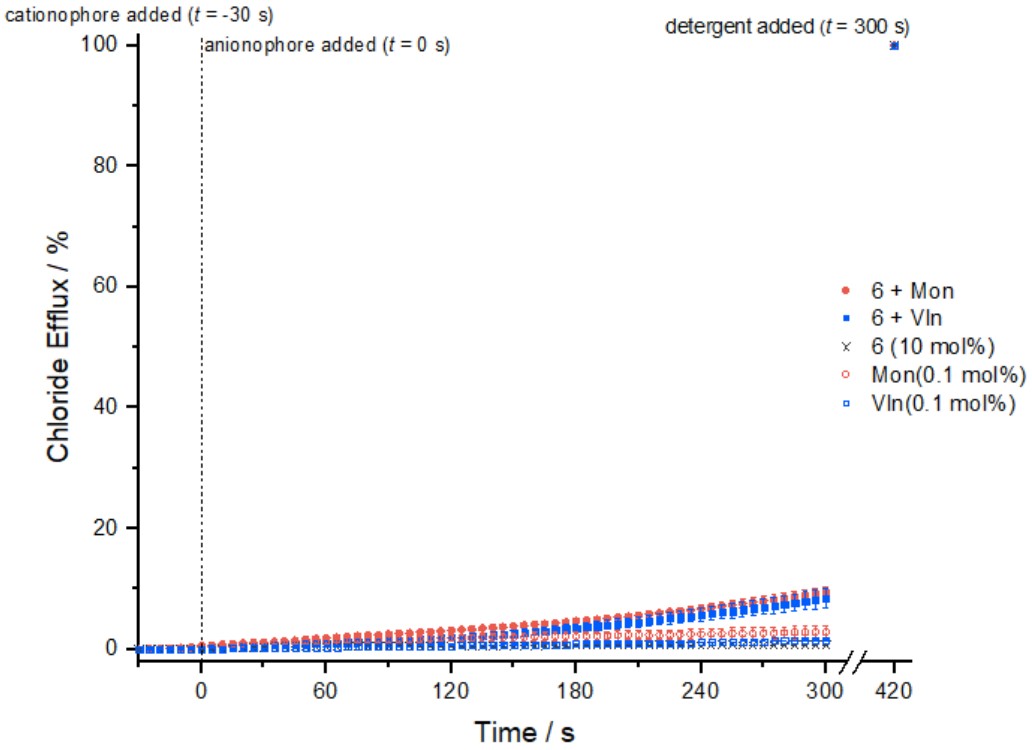

Fig. S49 Plot for chloride efflux mediated by compound **6** (10 mol%) in the presence of monensin and valinomycin at pH 4.5. Each data point represents the average of three repeat measurements with error bars indicating the standard deviation.

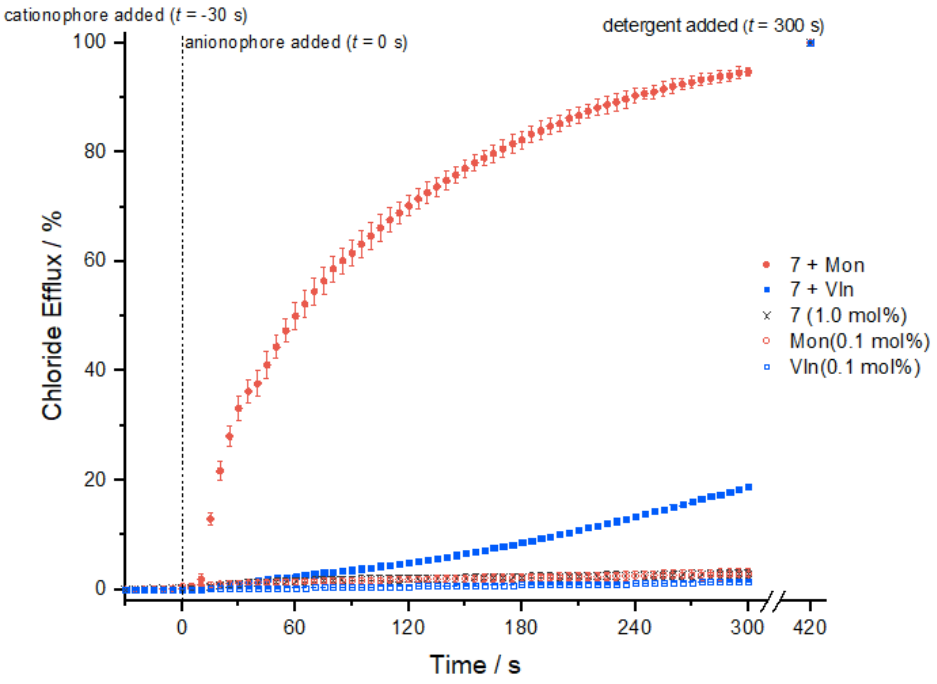

Fig. S50 Plot for chloride efflux mediated by compound **7** (1 mol%) in the presence of monensin and valinomycin at pH 7.2. Each data point represents the average of three repeat measurements with error bars indicating the standard deviation.

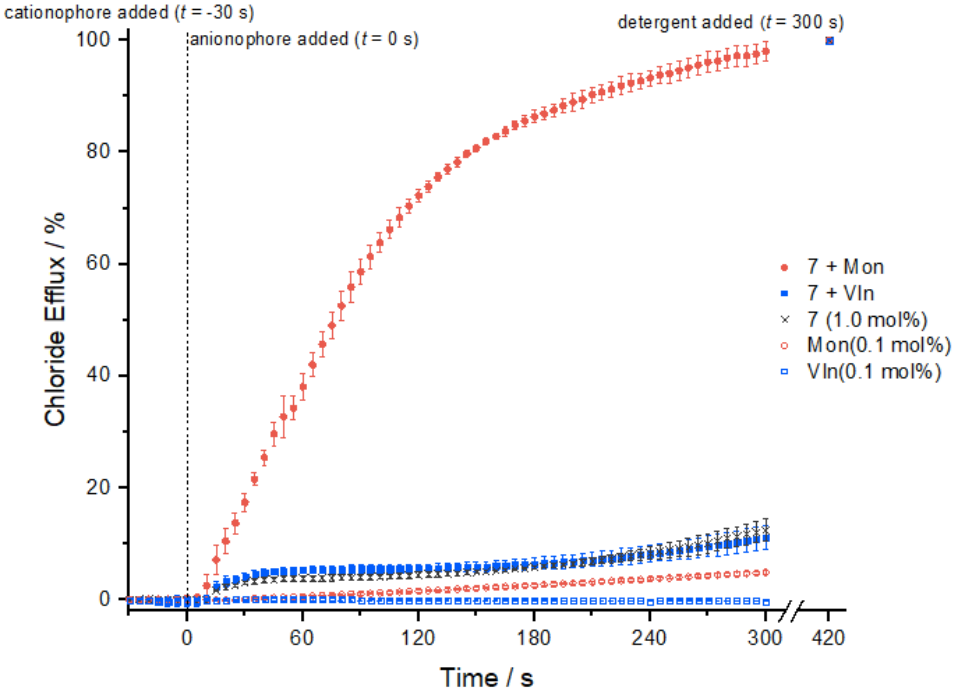

Fig. S51 Plot for chloride efflux mediated by compound **7** (1 mol%) in the presence of monensin and valinomycin at pH 4.5. Each data point represents the average of three repeat measurements with error bars indicating the standard deviation.

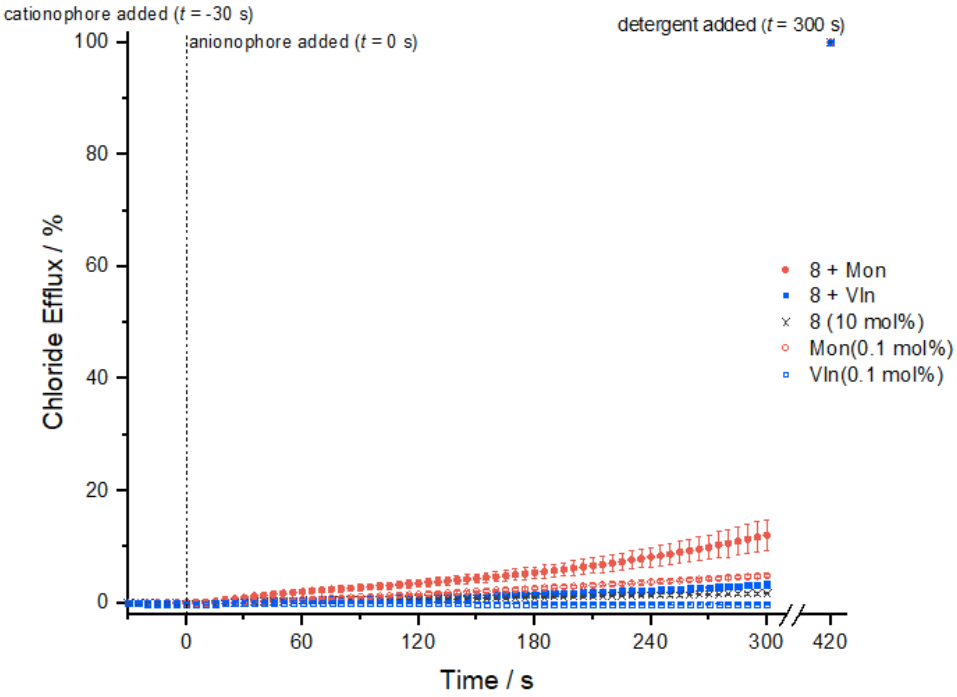

Fig. S52 Plot for chloride efflux mediated by compound **8** (10 mol%) in the presence of monensin and valinomycin at pH 7.2. Each data point represents the average of three repeat measurements with error bars indicating the standard deviation.

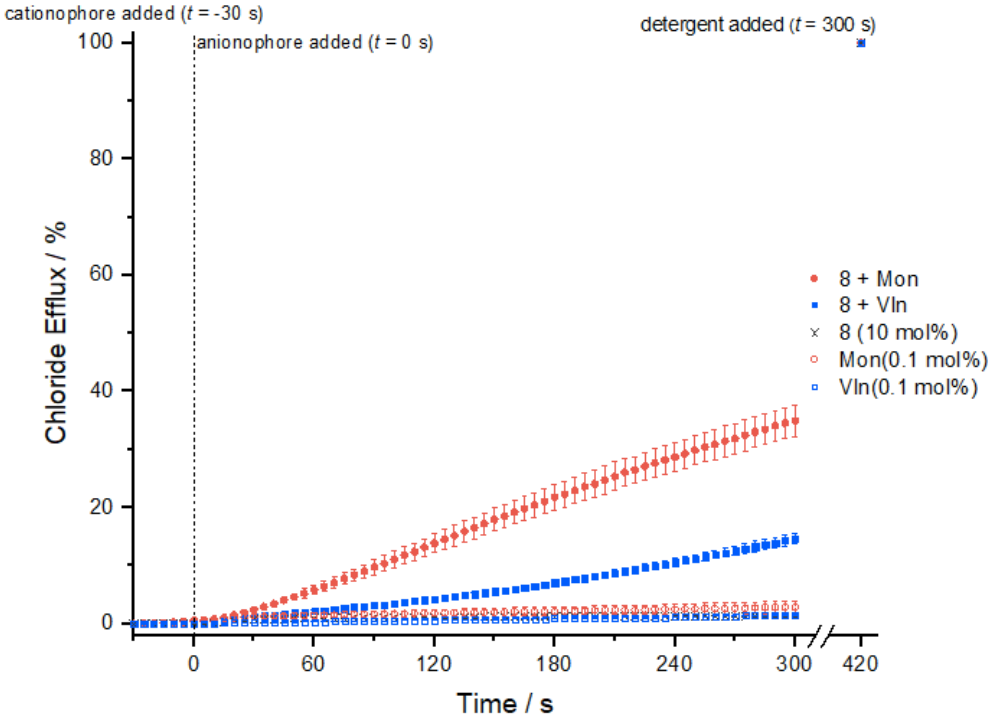

Fig. S53 Plot for chloride efflux mediated by compound **8** (10 mol%) in the presence of monensin and valinomycin at pH 4.5. Each data point represents the average of three repeat measurements with error bars indicating the standard deviation.

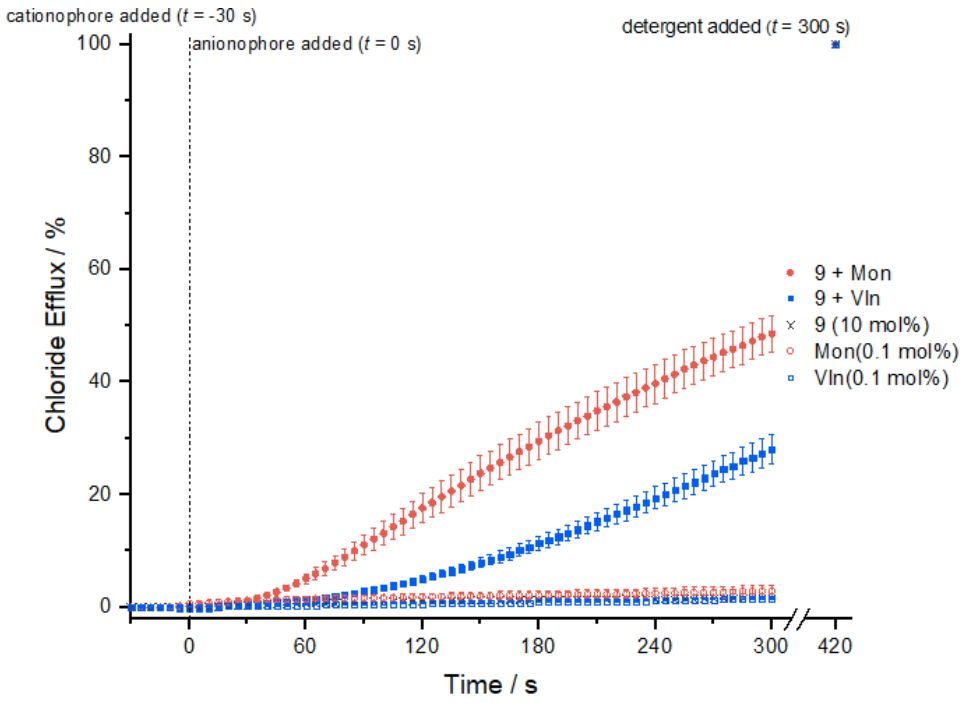

Fig. S54 Plot for chloride efflux mediated by compound **9** (10 mol%) in the presence of monensin and valinomycin at pH 7.2. Each data point represents the average of three repeat measurements with error bars indicating the standard deviation.

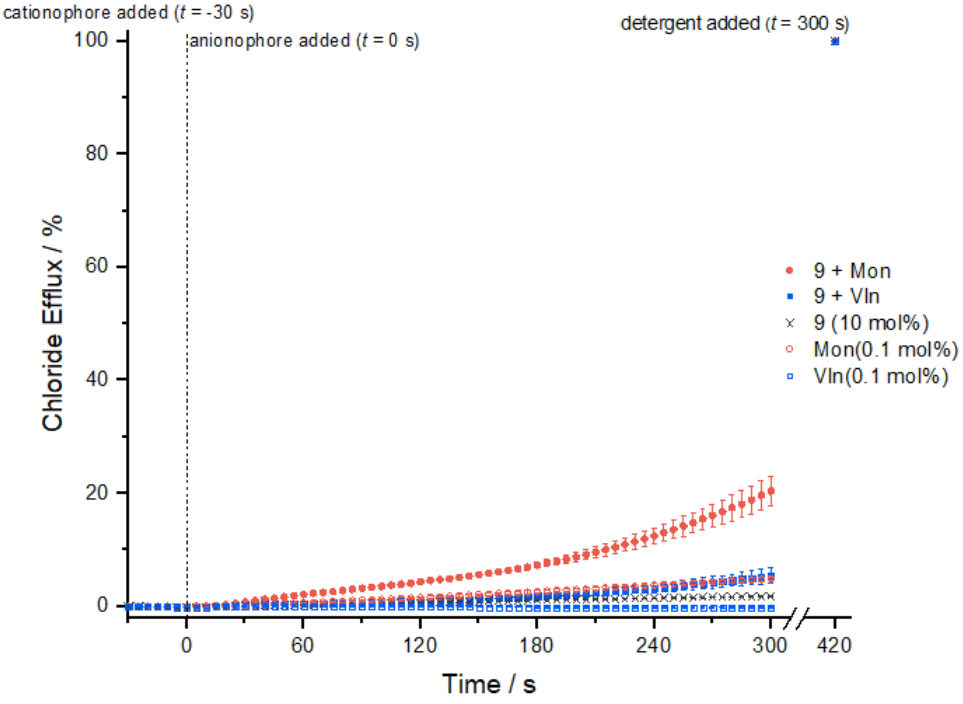

Fig. S55 Plot for chloride efflux mediated by compound **9** (10 mol%) in the presence of monensin and valinomycin at pH 4.5. Each data point represents the average of three repeat measurements with error bars indicating the standard deviation.

S2.6 Comparison of Cl^-/NO_3^- exchange and cationophore-coupled assay

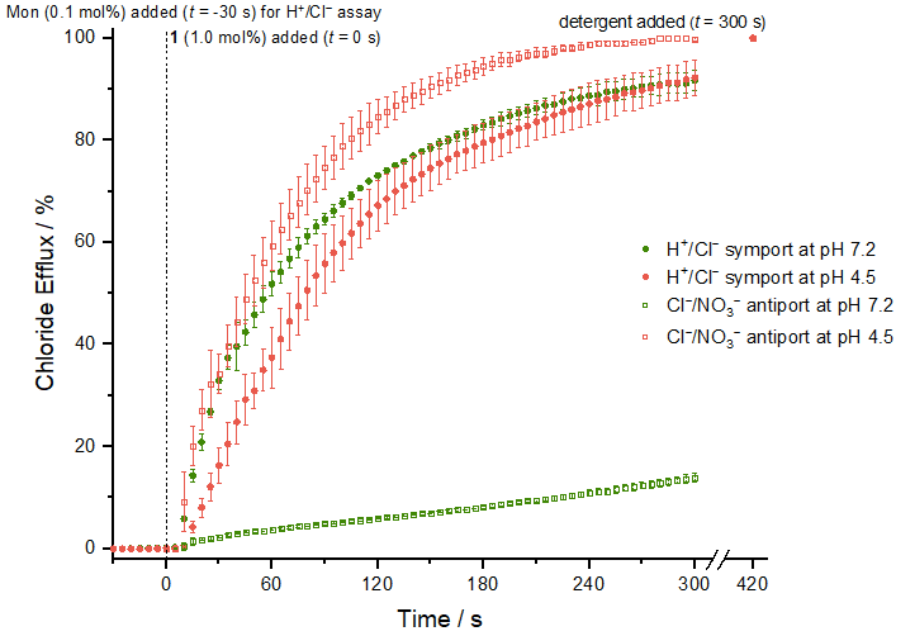

Fig. S56 Comparison plot for chloride efflux mediated by compound **1** (1 mol%) in the presence of monensin and valinomycin and Cl^-/NO_3^- exchange at pH 4.5 and 7.2. Each data point represents the average of two or three repeat measurements with error bars indicating the standard deviation.

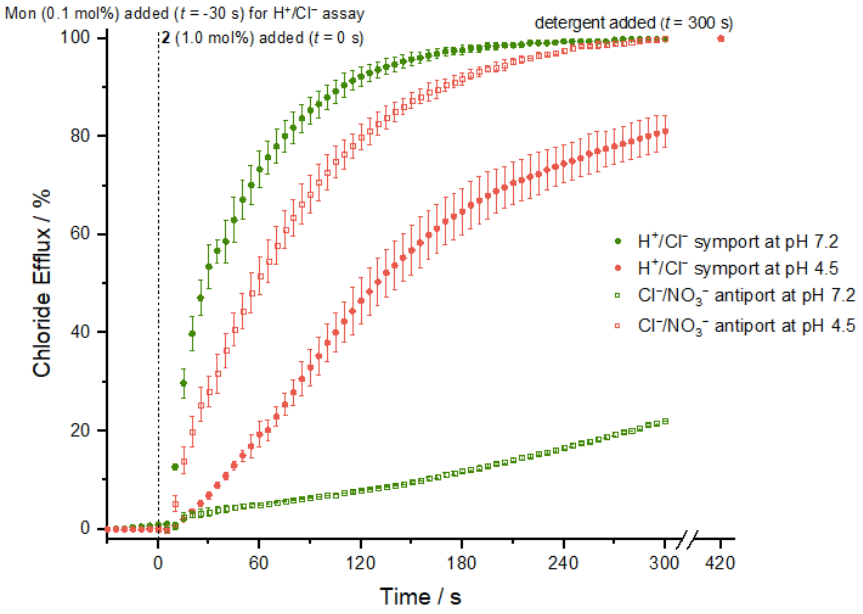

Fig. S57 Comparison plot for chloride efflux mediated by compound **2** (1 mol%) in the presence of monensin and valinomycin and Cl^-/NO_3^- exchange at pH 4.5 and 7.2. Each data point represents the average of two or three repeat measurements with error bars indicating the standard deviation.

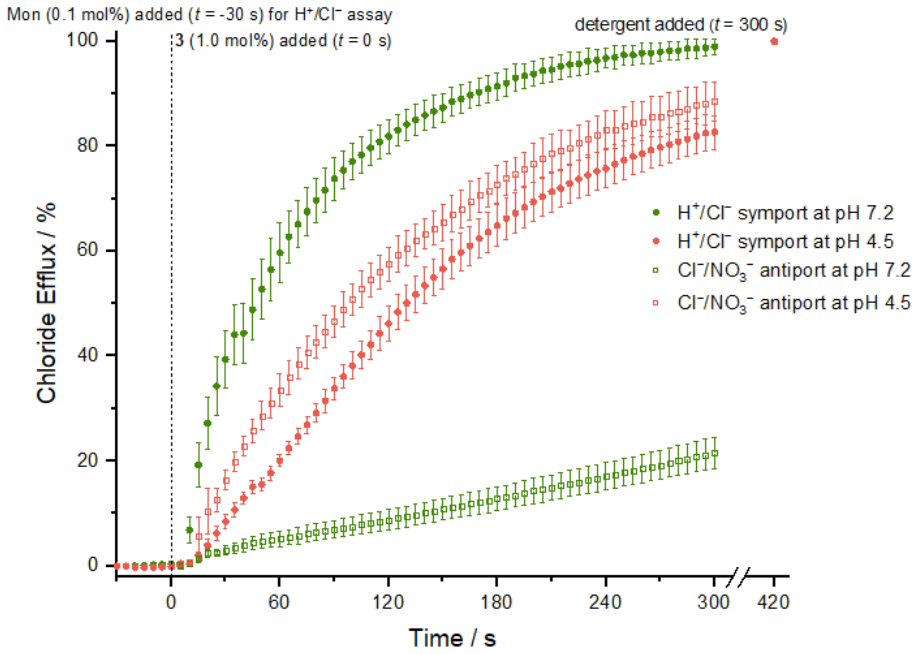

Fig. S58 Comparison plot for chloride efflux mediated by compound **3** (1 mol%) in the presence of monensin and valinomycin and Cl^-/NO_3^- exchange at pH 4.5 and 7.2. Each data point represents the average of two or three repeat measurements with error bars indicating the standard deviation.

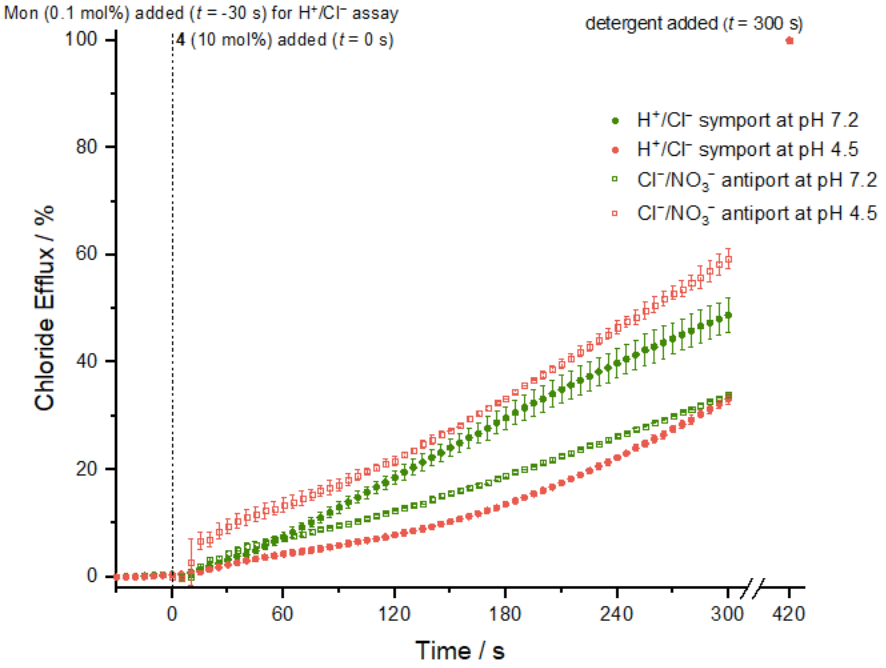

Fig. S59 Comparison plot for chloride efflux mediated by compound **4** (10 mol%) in the presence of monensin and valinomycin and Cl^-/NO_3^- exchange at pH 4.5 and 7.2. Each data point represents the average of two or three repeat measurements with error bars indicating the standard deviation.

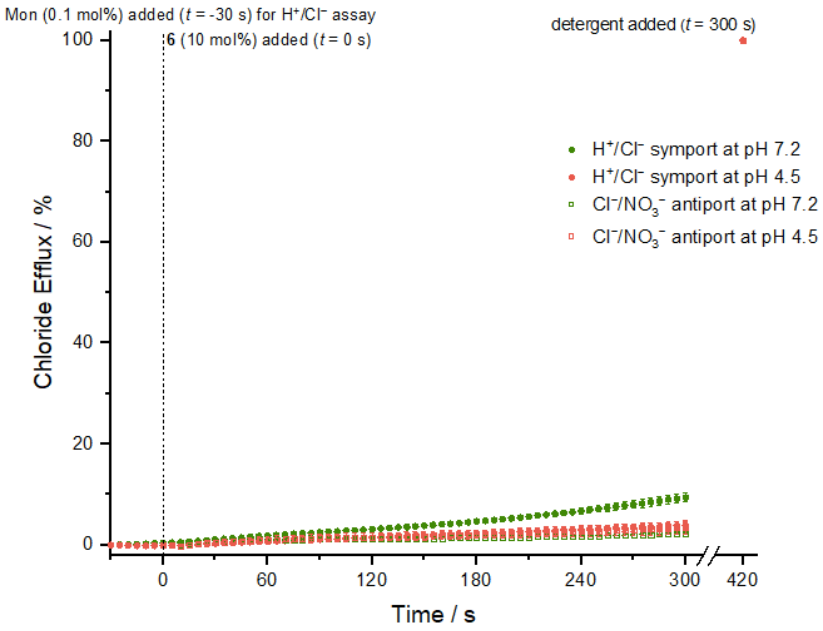

Fig. S60 Comparison plot for chloride efflux mediated by compound **5** (10 mol%) in the presence of monensin and valinomycin and Cl^-/NO_3^- exchange at pH 4.5 and 7.2. Each data point represents the average of two or three repeat measurements with error bars indicating the standard deviation.

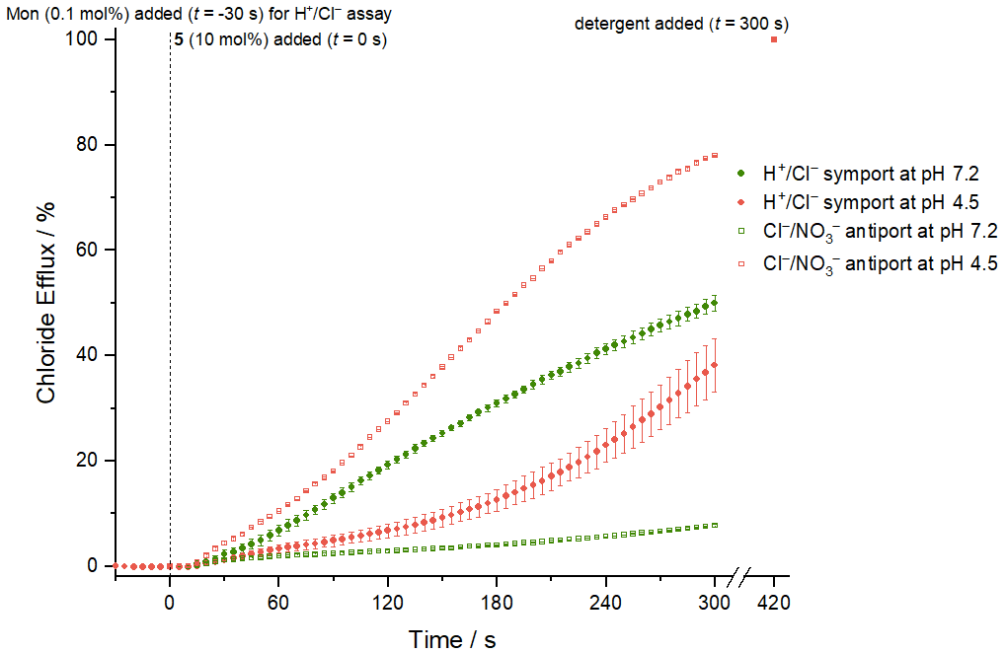

Fig. S61 Comparison plot for chloride efflux mediated by compound **6** (10 mol%) in the presence of monensin and valinomycin and Cl^-/NO_3^- exchange at pH 4.5 and 7.2. Each data point represents the average of two or three repeat measurements with error bars indicating the standard deviation.

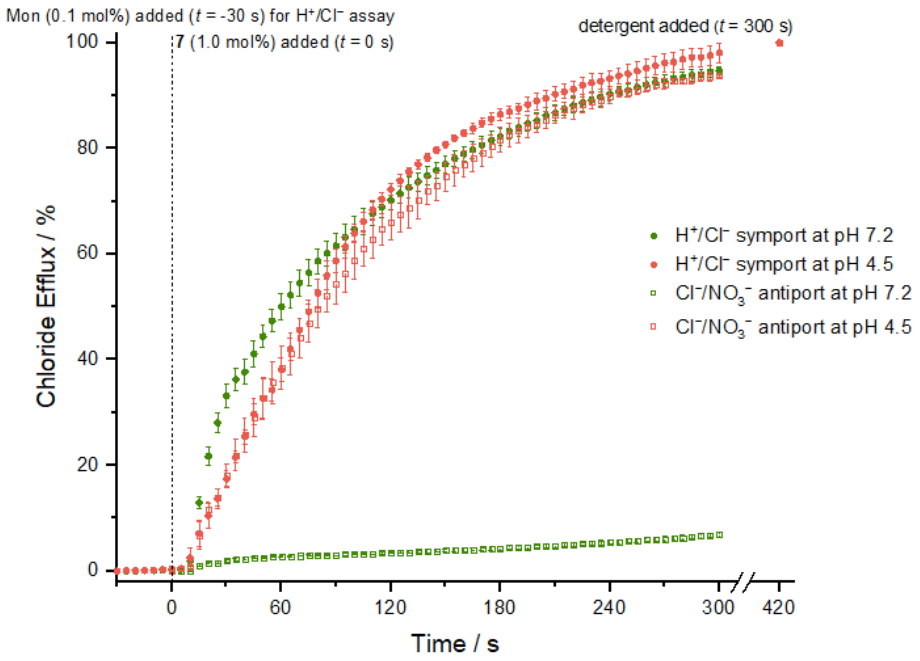

Fig. S62 Comparison plot for chloride efflux mediated by compound **7** (1 mol%) in the presence of monensin and valinomycin and Cl^-/NO_3^- exchange at pH 4.5 and 7.2. Each data point represents the average of two or three repeat measurements with error bars indicating the standard deviation.

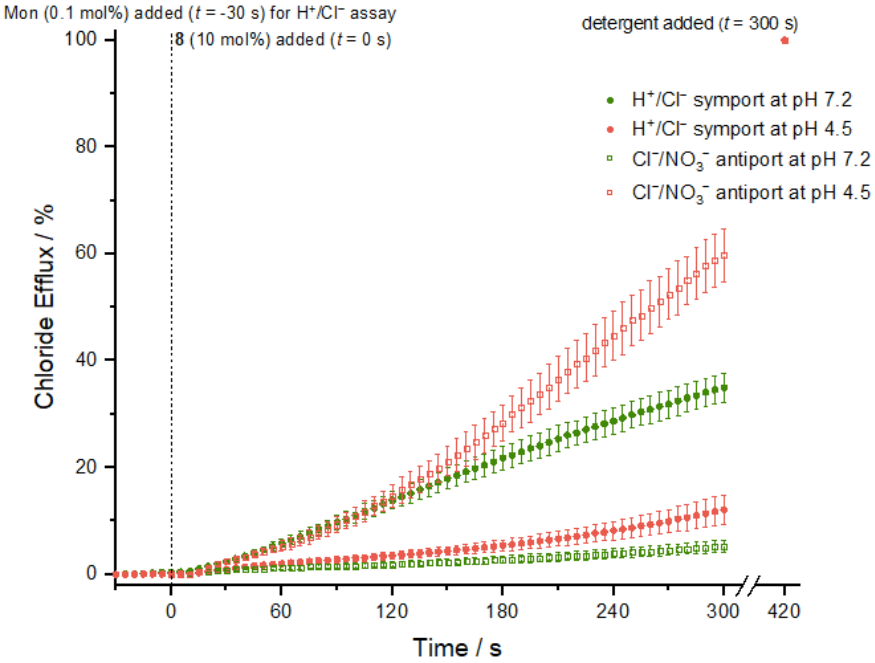

Fig. S63 Comparison plot for chloride efflux mediated by compound **8** (10 mol%) in the presence of monensin and valinomycin and Cl^-/NO_3^- exchange at pH 4.5 and 7.2. Each data point represents the average of two or three repeat measurements with error bars indicating the standard deviation.

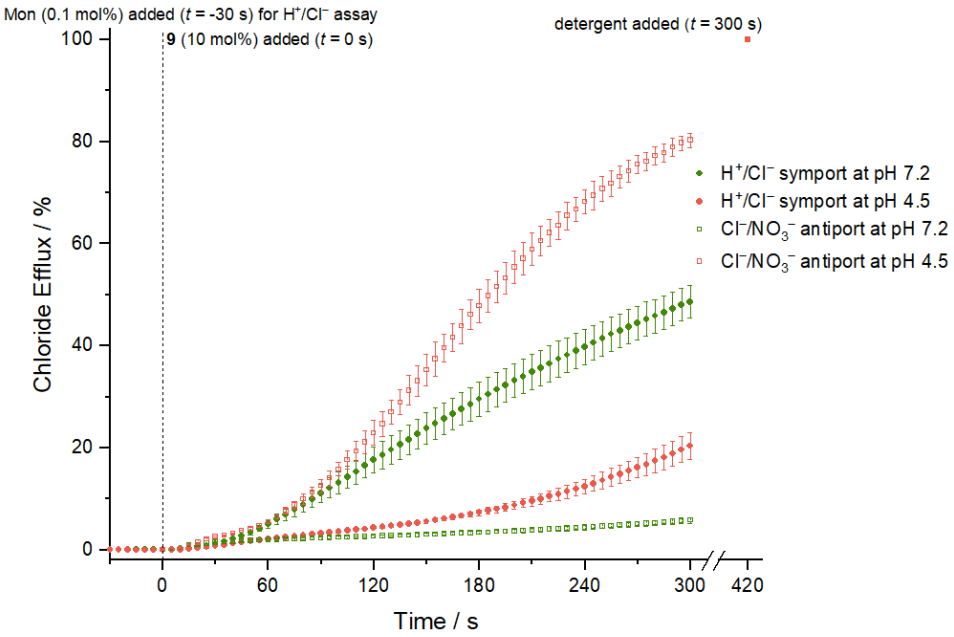

Fig. S64 Comparison plot for chloride efflux mediated by compound **9** (10 mol%) in the presence of monensin and valinomycin and Cl^-/NO_3^- exchange at pH 4.5 and 7.2. Each data point represents the average of two or three repeat measurements with error bars indicating the standard deviation.

S3 HPTS assay

S3.1 Vesicle preparation

HPTS assays[1] were conducted using POPC LUVs (mean diameter 200 nm) loaded with the pH-sensitive fluorescence dye HPTS (1 mM). The HPTS-loaded POPC LUVs were prepared as follows. A chloroform solution of POPC was evaporated in a round-bottom flask and the lipid film formed was dried under vacuum for at least 6 h. Then, the lipid film was hydrated by vortexing with an internal solution containing HPTS (1 mM) and NaX (100 mM, X = Cl^-, Br^-, NO_3^-, I^-, or ClO_4^-) buffered at pH 7.0 with 10 mM HEPES. The lipid suspension was subjected to nine freeze/thaw cycles and then extruded 25 times through a 200 nm polycarbonate membrane. The unentrapped HPTS was removed by a Sephadex G-25 column using an external solution of NaX buffered at pH 7.0 with 10 mM HEPES, to obtain NaX^{in}/NaX^{out} vesicle stock suspensions (with POPC concentration of ~10 mM).

S3.2 Anion gradient assay

Following vesicle preparation according to the general procedure, the NaCl-containing vesicles were diluted using NaX (100 mM) external solutions to obtain $NaCl^{in}/NaX^{out}$ vesicles suspended in 2.5 mL samples containing 0.1 mM of POPC. The samples were stirred at 298 K.

No base pulse was added so no pH gradient was initially present. Transporter **1** (added in 5 μL of DMSO) was added at time 0 to induce pH_{in} changes. The pH_{in} was monitored by the

ratiometric fluorescence response of HPTS I_{460} / I_{403} (λ_{ex} = 460 nm, λ_{em} = 510 nm divided by λ_{ex} = 403 nm, λ_{em} = 510 nm). The I_{460} / I_{403} values were converted to pH_{in} using previously reported calibration.

S3.3 pH gradient dissipation assay

Following vesicle preparation according to the general procedure, the NaX-containing vesicles were diluted using NaX (100 mM) external solutions to obtain NaX^{in}/NaX^{out} vesicles suspended in 2.5 mL samples containing 0.1 or 1.0 mM of POPC. The samples were stirred at 298 K.

A base pulse of NaOH (25 μL of 0.5 M NaOH solution, final concentration 5 mM) was added to the vesicle samples to generate a pH gradient with pH 7.0 inside and pH 8.0 outside vesicles. Subsequently, an anion transporter (added in 5 μL of DMSO) was added at time 0 and the rate of the pH gradient dissipation was monitored by the ratiometric fluorescence response of HPTS I_{460} / I_{403} (λ_{ex} = 460 nm, λ_{em} = 510 nm divided by λ_{ex} = 403 nm, λ_{em} = 510 nm). The I_{460} / I_{403} data were converted to fractional fluorescence (I_f) values using the following equation:

$$I_f = \frac{R_t - R_0}{R_f - R_0}$$

where R_t is the fluorescence ratio at time t, R_0 is the fluorescence ratio at time 0, and R_f is the fluorescence ratio after the addition of detergent.

We have previously shown that the I_{460} / I_{403} value, instead of the pH_{in}, is proportional to the amount of H^+ efflux.[2] Therefore, here for the purpose of indicating the progress of membrane transport, the I_{460} / I_{403} values were not converted to pH_{in} values.

S4 X-ray crystallography

Table S1. Crystal and data refinement parameters for the X-ray studies.

	1
CCDC Deposition number	2103182
Formula	C18 H21 N3 S
Formula weight	311.44
Temperature/K	100(2)
Crystal system	monoclinic
Space group	$P2_1/c$
a (Å)	10.43746(18)
b (Å)	13.7931(2)
c (Å)	23.7555(5)
B (°)	99.3315(17)
Volume (Å^3)	3374.69(11)
Z	8
ρ_{calc} /g cm^{-3}	1.226
μ (mm^{-1})	1.688
F (000)	1328
Reflections collected	13684
Independent reflections	[R_{int} = 0.0235, R_{sigma} = 0.0309]
Data/restraints/parameters	13684/0/411
GooF	1.063
Final R indexes [I>=2σ (I)]	R_1 = 0.0468, wR_2 = 0.1192
Final R indexes [all data]	R_1 = 0.0548, wR_2 = 0.1247
Largest diff. peak/hole / e Å^{-3}	0.505/−0.262

Table S2. Hydrogen-bonding parameters from the X-ray study of **1**.

Interaction	**H···A [A]^B**	**D···A [A]^B**	**D–H···A [°]^B**
N(2)···S(2)^1	2.52(3)	3.3644(17)	163(2)
N(8)···S(2)^1	2.97	3.7656(19)	142.5
C(5)···S(2)	2.84	3.677(2)	148.2
C(13)···N(6)	2.74	3.570(3)	146.3
N(5)···S(1)^2	2.64(3)	3.4939(17)	170(2)
C(26)···S(1)^2	2.99	3.8440(19)	149.7

[1] 1-X, ½ +Y, 3/2 -Z, [2] 1-X, - ½ +Y, 3/2 -Z

S5 References

1. S. Matile and N. Sakai, in *Analytical Methods in Supramolecular Chemistry*, ed. C. A. Schalley, Wiley-VCH, Weinheim, 2012, pp. 711-742.
2. H. J. Clarke, X. Wu, M. E. Light and P. A. Gale, *J Porphyr Phthalocya*, 2020, **24**, 473-479.